SULFUR TOLERANCE OF Fe PROMOTED BaO/Al_2O_3 SYSTEMS AS NO_x STORAGE MATERIALS

A THESIS
SUBMITTED TO THE DEPARTMENT OF CHEMISTRY AND
THE GRADUATE SCHOOL OF ENGINEERING AND SCIENCE
OF
BILKENT UNIVERSITY
IN PARTIAL FULFILLMENT OF THE REQUIREMENTS
FOR THE DEGREE
OF
MASTER OF SCIENCE

by

EMRAH PARMAK

AUGUST 2011

Aileme...

I certify that I have read this thesis and in my opinion it is fully adequate, in scope and quality, as a thesis of the degree of Master of Science

_____

Assistant Prof. Dr. Emrah ÖZENSOY (Supervisor)

I certify that I have read this thesis and in my opinion it is fully adequate, in scope and quality, as a thesis of the degree of Master of Science

_____

Prof. Dr. Deniz ÜNER

I certify that I have read this thesis and in my opinion it is fully adequate, in scope and quality, as a thesis of the degree of Master of Science

_____

Associate Prof. Dr. N. Alper TAPAN

Approved for the Graduate School of Engineering and Sciences

_____

Prof. Dr. Levent ONURAL

Director of the Graduate School of Engineering and Sciences

ABSTRACT

SULFUR TOLERANCE OF Fe PROMOTED BaO/Al_2O_3 SYSTEMS AS NO_x STORAGE MATERIALS

EMRAH PARMAK

M.S. in Chemistry

Supervisor: Assistant Prof. Dr. Emrah ÖZENSOY

August 2011

Ternary mixed oxide systems in the form of $BaO/FeO_x/Al_2O_3$ were studied with varying compositions as an alternative to the conventional NO_x storage materials (i.e. BaO/Al_2O_3). NO_x uptake properties of the freshly prepared samples, sulfur adsorption and NO_x storage in the presence of sulfur were investigated in order to elucidate the sulfur tolerance of these advanced NO_x storage systems in comparison to their conventional counterparts.

The structural characterization of the poisoned NO_x storage materials was analyzed by means of scanning electron microscopy (SEM).

The performance and sulfur tolerance of these materials upon SO_x adsorption were monitored by in-situ Fourier transform infrared (FTIR) spectroscopy, temperature programmed desorption (TPD) and X-Ray Photoelectron Spectroscopy (XPS).

Addition of FeO_x domains to the conventional BaO/Al_2O_3 system was observed to introduce additional NO_x storage sites and tends to increase the total NO_x uptake capacity.

SO_2+O_2 adsorption on the investigated samples was found to lead to the formation of sulfites at low temperatures which are converted into surface and bulk sulfates with increasing temperatures. After annealing at 1173 K in vacuum most of

the sulfates can be removed from the surface and the samples can be regenerated. However, for Fe/Ba/Al samples formation of various highly-stable sulfite and sulfate species were also observed which survive on the surface even after annealing at elevated temperatures (1173 K).

Sulfur poisoning on 5(10)Fe/8Ba/Al samples leads to preferential poisoning of the FeO_x, Al_2O_3 and surface BaO sites where bulk BaO sites seems to be more tolerant towards sulfur poisoning. In contrast, sulfur poisoning occurs in a rather non-preferential manner on the 5(10)Fe/20Ba/Al samples influencing all of the NO_x storage sites.

Thermal stability of the sulfate species seem to increase in the following order: surface alumina sulfates < surface Ba sulfates ≈ Fe sulfates < bulk Ba sulfates ≈ bulk alumina sulfates < highly stable sulfates and sulfites on Fe/Ba/Al surfaces.

In overall, it can be argued that the Fe promotion has a positive influence on the NO_x storage capacity as well as a positive effect on the sulfur tolerance when the Ba loading is equal to 8 wt% (i.e. 5(10)Fe/8Ba/Al). For these samples, even the surface uptakes more SO_x than conventional 8Ba/Al system, NO_x uptake properties as well as thermal regeneration properties seem slightly improved. On the other hand, for higher Ba loadings (i.e. 5(10)Fe/20Ba/Al) Fe promotion has a minor positive effect on NO_x uptake capacity and SO_x tolerance for 5 wt% Fe promotion while 10 wt% Fe promotion seems to have no positive influence.

Keywords: NSR, NO_x storage materials, γ-Al_2O_3, Ba/Al, Fe/Ba/Al, SO_x poisoning, FTIR spectroscopy, TPD, XPS and SEM-EDX.

ÖZET

Fe İLE ZENGİNLEŞTİRİLMİŞ NO_x DEPOLAMA MALZEMESİ OLAN BaO/Al_2O_3 SİSTEMLERİNİN KÜKÜRT TOLERANSI

EMRAH PARMAK

Kimya Bölümü Yüksek Lisans Tezi
Tez Yöneticisi: Yard. Doç. Emrah ÖZENSOY
Ağustos 2011

Bu çalışmada, konvensiyonel BaO/Al_2O_3 NO_x depolama malzemelerine alternatif olarak değişik kompozisyonlara sahip üçlü oksit yapıdaki $BaO/FeO_x/Al_2O_3$ malzemeleri incelenmiştir. Konvensiyonel (BaO/Al_2O_3) malzemelere kıyasla kükürt toleranslarını incelemek için bu malzemelerin kükürt dioksit adsorpsiyonları, sülfür varlığındaki ve yokluğundaki NO_x depolama kapasiteleri çalışılmıştır.

Kükürt ile zehirlenmiş NO_x depolama malzemelerinin yapısal karakterizasyonları taramalı elektron mikroskobu (SEM) tekniği kullanılarak yapılmıştır.

Bu malzemelerin SO_x adsorpsiyonu sırasındaki/sonucundaki performansları ve kükürt zehirlenmesine toleransları Fourier Dönüşümlü Kızıl Ötesi Spektroskopisi (FTIR), sıcaklık programlı yüzeyden buharlaştırma (TPD) ve X-Işını Fotoelektron Spektroskopisi (XPS) ile izlenmiştir.

Konvensiyonel malzemelere FeO_x ilavesinin malzemelerin NO_x tutma ve depolama kapasitelerini arttırdığı gözlemlenmiştir.

İncelenen bu malzemeler üzerindeki SO_2+O_2 adsorpsiyonunun düşük sıcaklıklarda sülfit oluşumuyla ve artan sıcaklıkla birlikte sülfitlerin, yüzeydeki birimlere bağlanmış ve iyonik (oylumsal) sülfatlara dönüşümüyle sonuçlandığı bulunmuştur. Numunelerin vakum ortamında 1173 K dereceye ısıtılmasıyla

sülfatların çoğunluğunun yüzeyden uzaklaştırılabileceği ve malzemelerin rejenere edilebileceği görülmüştür. Bununla birlikte, Fe/Ba/Al malzemeleri yüzeyinde, çok kararlı, yüksek sıcaklarda bile (1173 K) yüzeyde kalan değişik sülfit ve sülfat oluşumları gözlemlenmiştir.

5(10)Fe/8Ba/Al numuneleri üzerindeki kükürt zehirlenmesinin tercihen FeO_x, Al_2O_3 ve yüzeydeki BaO birimlerinin zehirlenmesiyle sonuçlanmasına karşın iyonik (oylumsal) BaO birimlerinin kükürt toleranslarının daha fazla olduğu görülmüştür. Bu durumun aksine, 5(10)Fe/20Ba/Al numuneleri üzerindeki kükürt zehirlenmesi yüzey veya iyonik birimleri tercihi olmaksızın tüm NO_x depolama birimlerini etkilemiştir.

Sülfat türlerinin ısıl kararlılıklarının şu şekilde sıralandığı görünmektedir: Al_2O_3 birimlerine bağlanmış sülfatlar < BaO birimlerine bağlanmış sülfatlar ≈ Fe birimlerine bağlanmış sülfatlar < BaO üzerindeki iyonik (oylumsal) sülfatlar ≈ Al_2O_3 üzerindeki iyonik (oylumsal) sülfatlar < Fe/Ba/Al malzemelerinin yüzeylerindeki çok kararlı sülfatlar ve sülfitler.

Genel olarak, demir ile zenginleştirmenin, düşük miktarda Ba yüklenmiş numunelerin (5(10)Fe/8Ba/Al) NO_x depolama kapasitelerinde ve kükürt toleranslarında olumlu etki yaptığı söylenebilir. Öte yandan, bu numunelerin yüzeyleri konvensiyonel 8Ba/Al malzemelerine kıyasla daha fazla SO_x tutmuştur. Buna karşın, yüksek miktarda Ba içeren malzemelerde (5(10)Fe/20Ba/Al) ağırlıkça %5 Fe ilavesi NO_x depolama kapasitesinde ve kükürt toleransında olumlu etki gösterirken, ağırlıkça %10 Fe ilavesi olumlu hiçbir etki göstermemiştir.

Anahtar Kelimeler: NSR, NO_x depolama malzemeleri, γ-Al_2O_3, Ba/Al, Fe/Ba/Al, SO_x zehirlenmesi, FTIR spektroskopisi, TPD, XPS and SEM-EDX.

ACKNOWLEDGEMENT

I would like to express my gratitude to…

My supervisor Assistant Prof. Dr. Emrah Özensoy for his guidance, encouragement, patience and supervision throughout my studies.

Evgeny Vovk, Zafer Say and Aslı Melike Soylu for their partnership and help during this research.

My group members Emre Emmez, Göksu Seda Şentürk and Cemal Albayrak, Mustafa Fatih Genişel, Hüseyin Alagöz, Ebru Devrim Şam and Zekury for their valuable friendship.

My parents; Nesibe and Hakkı and my brother Murat for their continuous love.

TABLE OF CONTENTS

LIST OF TABLES

LIST OF FIGURES

1 INTRODUCTION

Air pollution, one of the most important environmental problems, mainly originates the emission of pollutants such as hydrocarbons (HC), carbon monoxide (CO), nitrogen oxides (NO_x) and sulfur oxides (SO_x) formed during the combustion of fossil fuels. With the huge amount of fossil fuel utilized during the last decades, it is crucial to take precautions and convert their post-combustion products into harmless chemicals [1].

Since the oil reserves are limited and the global energy demand is constantly increasing, it is inevitable to search for solutions to minimize the consumption of fossil fuels in the automobile sector. The lean burn engine became a promising technology due to its fuel economy. It operates at an air-fuel (A/F) ratio of 25/1; in contrast to 14.5/1 for the conventional gasoline engines [2].

NO_x emissions have harmful effects on health and the environment. In Europe by the end of 2014, NO_x emissions from diesel engines are required to go through a three-fold decrease from 0,25 $g.km^{-1}$ to 0,08 $g.km^{-1}$ as mentioned in the EURO 6 AECC regulations named as the "Emission Control Technologies and the Euro 5/6 Emission Legislation" [3]. New technologies, therefore, are need for the reduction of NO_x emissions to satisfy these upcoming restrictions.

Various exhaust emission control technologies exist to control harmful emissions. For instance three–way catalaysts (TWCs) are generally composed of a high-surface area support material (i.e. γ-Al_2O_3) and nobel metals such as Pt-Rh and/or Pd/Rh, functioning as active sites for the removal of harmful gas, in addition to other promoters and enhancers [4]. Although TWCs have proved to be efficient and reliable for gasoline-engine applications, they are ineffective for NO_x reduction in lean-burn engine systems [5]. In Figure 1, it can be seen that a typical TWC can perform well at an A/F ratio of 14.5/1, whereas at an A/F ratio of 25/1 it severely fails to perform NO_x reduction.

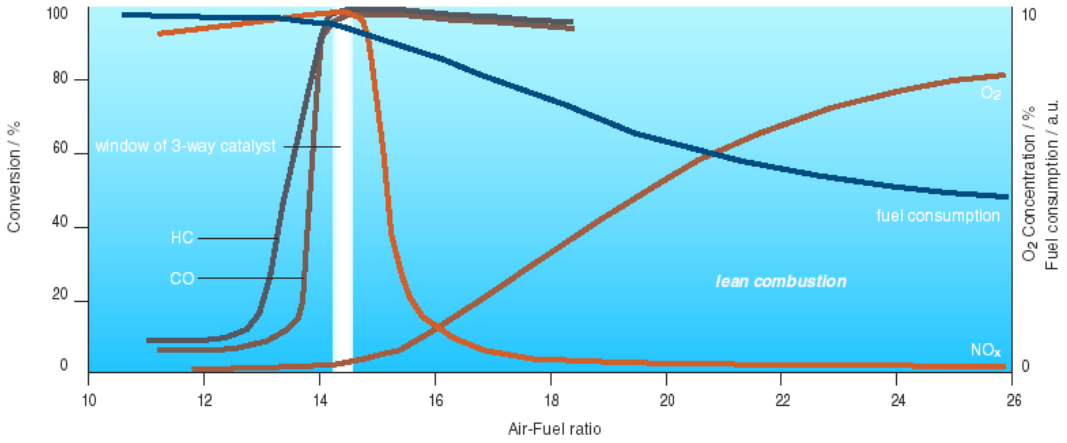

Figure 1. Fuel consumption and three-way performance of a gasoline engine as a function of air–fuel (A/F) ratio [6].

Therefore, new catalysts are needed for lean-burn engines to meet the NO_x emission standards. There are two other alternative technologies used for this purpose; one of which is the selective catalytic reduction (SCR) and the other is NO_x Storage and Reduction (NSR) technology.

There are two main types of SCR catalysts; ammonia/urea selective catalytic reduction catalysts (NH_3-SCR) and hydrocarbon selective catalytic reduction catalysts (HC-SCR) [7]. NH_3-SCR has the disadvantage of having corrosive and toxic NH_3; moreover, NH_3 may react with NO_2 resulting in the formation of explosive ammonium nitrate causing the deactivation of catalyst [8]. HC-SCR catalysts, based on zeolites, are also used to remove NO_x under A/F ratio of 25/1; however, they have the drawbacks such as not being active at low temperatures and being deactivated by water and SO_2 [9].

Another different concept to reduce NO_x under high A/F ratio is NO_x Storage and Reduction technology [10]. A typical NSR catalyst is built on three parts; a support material such as γ-Al_2O_3, a storage component such as an alkaline-earth oxide (BaO) and supported precious metal such as Pt, Pd and Rh [11].

NSR catalysts follow two different regimes while operating; the long (lean) regime which is oxygen-rich and the short (rich) regime that is oxygen deficient [9]. As can be seen from Figure 2, during the long (lean) regime, NO is oxidized to NO_2 and then stored as NO_x in the storage material and during the short (rich) regime

these NO_x species is released from the storage component and reduced to N_2 by reducing atmosphere (hydrocarbons) [12].

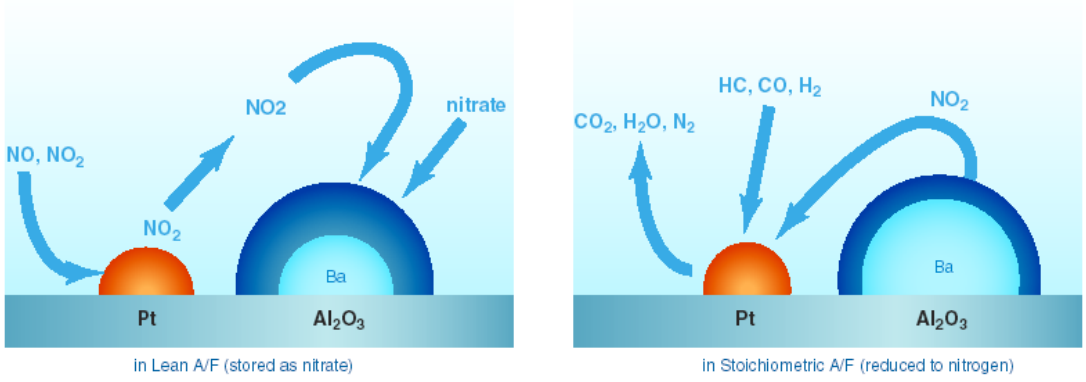

Figure 2. A simplified representation of the NO_x storage-reduction on the NSR catalyst [13].

For a better understanding of the complexity of the NO reduction process, the following microkinetic model by Xu et al. [14] can be considered which focuses on NO reduction by H_2 on Pt :

$$NO + Pt \leftrightarrow NO - Pt$$
$$H_2 + 2Pt \leftrightarrow 2H - Pt$$
$$NO - Pt + H - Pt \leftrightarrow N - Pt + OH - Pt$$
$$N_2O + 2Pt \leftrightarrow NO - Pt + N - Pt$$
$$H - Pt + O - Pt \leftrightarrow OH - Pt + Pt$$
$$H - Pt + OH - Pt \rightarrow H_2O + 2Pt$$
$$2N - Pt \leftrightarrow N_2 + 2Pt$$
$$NO - Pt + Pt \leftrightarrow N - Pt + O - Pt$$
$$N_2O + Pt \leftrightarrow N_2 + O - Pt$$
$$N - Pt + H - Pt \leftrightarrow NH - Pt + Pt$$
$$NH - Pt + H - Pt \leftrightarrow NH_2 - Pt + Pt$$
$$NH_2 - Pt + H - Pt \leftrightarrow NH_3 - Pt + Pt$$
$$NH_3 + Pt \leftrightarrow NH_3 - Pt$$
$$O_2 + 2Pt \leftrightarrow 2O - Pt$$
$$NO - Pt + O - Pt \leftrightarrow NO_2 - Pt + Pt$$
$$NO_2 + Pt \leftrightarrow NO_2 - Pt$$

As can be seen from this particular model, the main products in the system are NO_2, N_2O, NH_3, N_2 and H_2O. From the first step until the sixth step (where the temperature is between 50 ^{0}C and 150 ^{0}C), N_2O is the main product. Adsorbed NO reacts with adsorbed hydrogen atoms, results in breakage of the NO bond. The N and OH adatoms react with NO and H respectively and N_2O and H_2O form. Above 200 ^{0}C, the rate of NO bond scission (eighth step) increases leading to an increase in N_2 production via seventh step. The formation of NH_3 is observed to be dependent on the H_2/NO ratio. Steps ten to thirteen correspond to the reversible hydrogen addition leading to the NH_3 formation. These steps are reversible due to decomposition of NH_3 at temperatures higher than 350 ^{0}C. Fourteenth, fifteenth and sixteenth steps are for adsorption-desorption of molecular oxygen, formation and adsorption of NO_2, respectively. This model does not consider the O_2 in the feed, since surface oxygen produced by the decomposition of NO reacts rapidly with the adsorbed H atoms in rich feed where H_2 concentration surpasses the NO concentration [14].

Alkaline and alkaline-earth metal oxides are significant for the storage of NO_2 due to their basic surface character [15]. Moreover, it is known that the adsorption properties of NO_x are related to the surface basicity of the substrate and the storage material. As the lattice parameter increases, the electrostatic stabilization of the ionic charge separation decreases while the basicity increases [16]. The Ba content in the catalyst has a direct influence on the stored NO_x; however, increasing of the Ba content in the catalyst beyond 20 wt. % is observed to have no positive effect on the amount of stored NO_x species. This may be due to the fact that that increasing the amount of Ba above 20 wt% may block available Pt sites or higher barium loading may decrease Pt dispersion on the surface [17].

Some of the commonly used precious metal components in NSR catalysts are Pt, Pd and Rh. Pt was observed to improve the adsorption of NO_2 by producing stable nitrates on the catalyst surface [18]. γ-Al_2O_3 is frequently used as the main NSR catalyst support material, because of its porous structure, high surface area, high catalytic surface activity, distinctive chemical, mechanical and thermal properties. [19].

One of the major drawbacks related to the NSR catalysts is catalytic deactivation and catalytic aging. Thermal aging, which is due to the reaction of the storage material with the support material and the associated morphology changes of

the precious metal and the storage material, is one of the sources of deactivation. Another important source for the deactivation of NSR catalysts is the sulfur poisoning. Despite the constant reduction in the sulfur content of the refined fuel in the past decades, sulfur poisoning remains one of the major causes for catalytic deactivation of the NSR systems [20].Sulfur present in diesel fuel produces SO_x during combustion and these SO_x species block storage sites during lean-burn conditions as a result of which barium sulfates and aluminum sulfates are formed. Because of high thermal stability of these sulfates, it is challenging to regain the storage capacity of the catalyst [20]. Moreover, formation of alumina sulfate limits the nitrate diffusion on the surface of support and clogs the pores of the support material [10]. Thus, for the widespread usage of NSR catalysts, it is crucial to promote the catalytic tolerance against sulfur poisoning.

The typical way of improving the catalytic tolerance against sulfur poisoning and designing highly active and stable novel catalysts is incorporating promoters (e.g. Ti, Fe, Cu) into Ba-based NSR catalysts. Matsumoto et al. investigated TiO_2 addition to the alumina catalyst, leading to a decrease in the amount of stored sulfate without a significant decrease in the NO_x storage capacity; therefore, it is demonstrated that the smaller the size of the sulfate particles, the easier the sulfate decomposition [21]. They also stated that the geometrical structure of the catalyst monolith plays a role on the size of the sulfate particles [21].

Tanaka et al. studied a Ba–Ti composite oxide where it was found that the formation of the Ba–Ti composite oxide on the NSR catalyst enhanced the sulfur desorption efficiency and led to efficient NOx conversion and reduction activity even after sulfation/regeneration cycles. It was proposed that the existence of nano-scaled Ba domains containing Ti was efficient for the inhibition of the sintering of barium sulfate and its facile decomposition. Hence, it was reported that the dispersion of Ba compounds for NO_x storage materials using a Ba–Ti mixed oxide is an efficient way to improve the durability of NSR catalysts [22].

Wang et al. developed a new $Cu/K_2Ti_2O_5$ catalyst to remove NO_x through the NSR process. The sulfur tolerance of this type of catalyst was suggested to arise from the inability of Cu to oxidize SO_2. It was found that the thermal stability of the adsorbed SO_x species on the oxygen vacancies is much less than that of the alkali/alkaline earth sulfate salts ($BaSO_4$, K_2SO_4, etc.) [23].

Basile et al. prepared a set of catalysts to improve the activity of the Ba-Pt/γ-Al_2O_3 catalyst, by replacing Ba with Mg or Ca.. They found that Mg-Ba-Pt/γ-Al_2O_3 catalyst shows an increase in both the NO_x storage-reduction capacity and the resistance to the deactivation by SO_2. This behavior was attributed to synergetic effects between the two storage components (i.e. Ba and Mg) which suppress the formation of crystalline $BaCO_3$ phases [24].

There are also a number of studies related to mixed oxides containing TiO_2 and ZrO_2 [25], $BaSnO_3$ [26], and Li_2O [27] on γ-Al_2O_3 which will not be discussed here.

Fe promotion of Pt/Ba/Al_2O_3 NSR system is a promising alternative for sulfur removal. An important effort to improve sulfur resistance by the addition of Fe promoters to the Pt/Ba/Al_2O_3 NSR system was made by Yamazaki et al [28]. They found that incorporation of Fe into the system did not influence the NO_x conversion in a significant manner. They also reported that the sulfur content of the Pt/Ba/Fe/Al_2O_3 catalyst exposed to a reducing gas (the simulated reducing gas consisted of 0.15% NO, 0.5% O_2, 0.1% C_3H_6, 1.4% CO, 10% CO_2, 3.0% H_2O) is about one-half of that of the Pt/Ba/Al_2O_3 catalyst exposed to the same gas. Moreover, they investigated the desorption profile of SO_2 from Pt/Ba/Fe/Al_2O_3 and Pt/Ba/Al_2O_3 catalysts as a function of Fe loading and observed that SO_2 desorption from the Pt/Ba/Fe/Al_2O_3 catalyst occurs at a lower temperature compared to that from the Pt/Ba/Al_2O_3 catalyst. It was also shown that SO_2 desorption temperature was lowered as the Fe loading increased which indicates that the Fe addition promotes the SO_2 desorption from the NSR catalyst. Another important outcome of their study was that the average size of the $BaSO_4$ particles on the Pt/Ba/Fe/Al_2O_3 catalyst was smaller than that of Pt/Ba/Al_2O_3 catalyst and the size of $BaSO_4$ particles decreased with increasing Fe loading [28].

Fanson et al. also studied Pt/Ba/Fe/γ-Al_2O_3 NSR catalysts [29]. After a prolonged exposure to SO_2, Pt/Fe/Ba/Al_2O_3 catalyst was found to preserve its NO_x storage capacity unlike the Pt/Ba/Al_2O_3 catalyst. However Pt/Fe/Ba/Al_2O_3 catalyst demonstrated a lower initial NO_x storage capacity in comparison to that of Pt/Ba/Al_2O_3. They concluded that after a long exposure to SO_2, although most of the conventional BaO sites have been converted into $BaSO_4$, sulfur resistant NO_x storage sites in the iron containing phase remained available for NO_x storage [29].

Hendershot et al. [30] argued that Fe promoted NSR system had a lower NO_x storage capacity compared to the NSR system which does not contain Fe and it was claimed that performance of these catalysts strongly depends on the catalyst preparation procedures. In another report, Hendershot et al. stated that the Fe did not significantly affect the poisoning of the Pt sites, and therefore the overall NO_x storage capacity and resistance to SO_2 was not significantly improved by the addition of Fe [31]. N. Le Phuc et al. [32] observed that Fe addition to the Pt-Ba-Al_2O_3 NSR system leads to deactivation rising from the interaction between Fe and Pt.

The NO_x storage property and sulfur resistance ability of the Fe-Ba-O mixed oxide was studied by Li et al. [33]. It was shown that Fe-Ba-O mixed oxide has a high NO_x storage capacity (comparable with Pt/Ba/Al_2O_3 NO_x storage capacity) and high sulfur resistance. Xian et al. synthesized noble metal free perovskite-type $BaFeO_{3-x}$ for NSR applications [34]. They demonstrated that NO_x storage capacity is enhanced due to transfer of the nitrates on the perovskite to the neighboring carbonate (which are formed during the synthesis) creating monodentate nitrates and regenerating the NO_x storage sites on the perovskite [34]. It is also stated that the iron atoms surrounding the barium atoms closely in the crystal lattice of the perovskite inhibit the sulfation of the barium, inducing a high sulfur tolerance [34]. In another study Shen et al. [35] investigated the effect of Fe addition to Mn-Ce/TiO_2 catalyst. It was reported that Fe doped Mn-Ce/TiO_2 catalyst exhibits higher NO_x reduction activity compared to the Mn-Ce/TiO_2. Apart from providing 96.8% NO conversion, Fe doped catalyst showed better resistance to SO_2 and H_2O. Rodriguez et al. [36] studied SO_2 interaction with Fe doped MgO and they observed that SO_2 dissociates on the surface of $Fe_xMg_{1-x}O$ upon adsorption whereas the interaction of Mg cations with SO_2 does not lead to cleavage of S-O bond.

To understand the structure of different sulfur containing species formed by the adsorption of SO_2 on Fe sites, the SO_2 interaction with iron oxides was investigated by IR spectroscopy. Fu et al. studied the heterogenous oxidation of gas-phase SO_2 on different Fe oxides [37]. They monitored SO_2 uptake on α-Fe_2O_3 (hematite) in the presence of O_2. In DRIFT spectra, negative bands within 3750 - 3150 cm^{-1} and 1700 -1500 cm^{-1}, were attributed to surface hydroxyl species, suggesting that the surface OH groups may be the active sites for SO_2 adsorption [37]. Three peaks with increasing intensities until the saturation of the surface were

observed at 1225, 1149, and 1042 cm^{-1} which were assigned to splitted ν_3 band of adsorbed bisulfate (HSO_4^-) and/or sulfate (SO_4^{2-}). The splitting of this band into three peaks (ν_3 is normally triply degenerate asymmetric streching mode) indicates that SO_2 symmetry is reduced and SO_2 is transformed into sulfates on the surface of the oxide. In contrast, no significant formation of sulfate was reported on the surface of α-Fe_2O_3 in the absence of O_2, suggesting that the concentration of adsorbed oxygen over catalyst surfaces may be the basic factor contributing to the oxidation. SO_2 was reported to bind to the surface through two oxygen atoms, resulting in the formation of the bidentate-surface complexes. Moreover, when Fe_3O_4 was exposed to SO_2, they observed three absorption bands between 1000 - 1300 cm^{-1} indicating the formation of bidentate sulfato-metal surface complexes. The XPS analysis of α-Fe_2O_3 exposed to SO_2 demonstrated the formation of SO_3^{2-} and SO_4^{2-} as well as Fe (III) and Fe (II) species. A similar result was also reported for Fe_3O_4 although with a different total SO_x uptake [37].

Baltrusaitis et al. [38] also investigated the adsorption of SO_2 on α-Fe_2O_3 (hematite) with XPS. They reported the formation of SO_3^{2-} at the initial exposure of SO_2 in the absence of oxygen, in addition, the presence of ferrous and ferric sulfates was detected on the surface of hematite. In the absence of O_2, the quantity of SO_4^{2-} species was negligible (SO_4^{2-}/ SO_3^{2-}, = ~ 1/10). On the other hand, in the presence of oxygen, dramatic changes on the relative distribution of sulfur species on hematite surface were observed: the predominant sulfur species was stated to be sulfates. Moreover, in the presence of oxygen, the uptake of SO_2 was observed to increase more than two times relative to experiments without oxygen.

In another study, Decyk et al. [39] investigated the poisoning effect of SO_2 on NO reduction over Fe/ZSM-5 catalyst. They studied the adsorption of SO_2 on Fe/ZSM-5 by means of TPD and found two peaks at 393 K and 900 K which were attributed to physically adsorbed SO_2 and the decomposition of sulfate and/or sulfite species on the surface respectively. They also reported that S2p photoelectron spectrum of SO_2 treated Fe/ZSM-5 indicates the formation of sulfate species such as $FeSO_4$. On the other hand, they did not observe any XPS peaks corresponding to sulfides or elemental sulfur. It is also shown that EPR (electron paramagnetic resonance) signals arising from the distorted tetrahedral Fe^{3+} ions, which are active sites, are disappeared after the poisoning of Fe/ZSM-5 with SO_2. Decyk et al. also

studied the effect of sulfur poisoning on the formation of NO_x species on Fe/ZSM-5 [39]. They reported the formation of nitro-, nitroso- and nitrate species after the adsorption of NO and O_2; however, it was observed that signals corresponding to nitro- and nitrate species disappeared after preadsorption of SO_2 followed by the adsorption of NO and O_2 mixture. In addition, new band at 1355 cm^{-1} in IR spectra is appeared, demonstrating sulfate formation. Thus, it was shown that the formation of Fe-NO_x is suppressed by the deactivation of Fe/ZSM-5 with SO_2 [39].

In the current study, interaction of SO_x (SO_2+O_2) with Fe promoted Ba/Al_2O_3 storage materials as well as SO_x poisoning effect on NO_x (NO+O_2) adsorption was carefully investigated with the help of the following methods: Fourier transform infrared (FTIR) spectroscopy was used for the characterization of the adsorbed species; Temperature programmed desorption (TPD) was used for thermal stability monitoring; X-ray photoelectron spectroscopy (XPS) was used for quantitative surface elemental analysis; Scanning electron microscopy (SEM) and Energy dispersive X-ray mapping (EDX-mapping) were used for surface morphology analysis of the investigated samples.

2 EXPERIMENTAL

2.1 Sample preparation

Four different NO_x storage materials in the form of Fe/ Ba/ γ-Al_2O_3 were synthesized with different loadings of Ba (8 and 20 wt. % BaO) and Fe (5 and 10 wt. % Fe) by incipient wetness impregnation [28] of γ-Al_2O_3 (PURALOX, 200 m^2/g, SASOL GmbH, Germany). γ-Al_2O_3 support material was impregnated with aqueous solutions of barium nitrate (ACS Reagent, ≥99%, Riedel – de Haën) and , $Fe(NO_3)_3$. $9H_2O$ (iron (III) nitrate nonahydrate, ACS reagent, ≥98%, Sigma - Aldrich). The reason for choosing Ba content between 8 and 20 wt. % is that 8wt%BaO is not enough to form one monolayer on γ-Al_2O_3 surface, whereas 20wt%BaO is more than enough to form two monolayers on γ-Al_2O_3 surface [40]. Synthesized materials were dried at 353 K, followed by annealing in Ar atmosphere for 2 h at 923 K to decompose the nitrates.

Besides these samples, , 8wt%BaO/γ-Al_2O_3, 20wt%BaO/γ-Al_2O_3, 5wt%Fe/ γ-Al_2O_3 and 10wt%Fe/γ-Al_2O_3 were also synthesized by incipient wetness impregnation of γ-Al_2O_3 and used as reference materials [28]. Synthesized materials and their abbreviations used in the current text are shown in Table 1.

Table 1. Compositions of the synthesized materials.

Abbreviations	**BaO (wt%)**	**Fe (wt%)**	**Al_2O_3 (wt%)**
8Ba/Al	8	-	92
20Ba/Al	20	-	80
5Fe/Al	-	5	95
10Fe/Al	-	10	90
5Fe/8Ba/Al	7.6	5	87.4
10Fe/8Ba/Al	7.2	10	82.8
5Fe/20Ba/Al	19	5	76
10Fe/20Ba/Al	18	10	72

2.2 Experimental Techniques

2.2.1 FTIR

The system designed for FTIR, RGA and TPD experiments is shown in Figure 3 [41]. FTIR spectroscopic measurements were performed in transmission mode in a batch-type catalytic reactor coupled to an FTIR spectrometer (Bruker Tensor 27) and a quadruple mass spectrometer (QMS) (Stanford Research Systems, RGA 200) for TPD and residual gas analysis (RGA). FTIR spectra were recorded with a Hg-Cd-Te (MCT) detector, where each spectrum was acquired by averaging 128 scans with a spectral resolution of 4 cm^{-1}. The samples were mounted into the IR cell consisting of a five-way stainless steel chamber equipped with optically-polished BaF_2 windows. This IR cell was connected to a gas manifold (including a dual-stage rotary vane pump and two turbomolecular pumps) so that the pressure in the cell could be varied within 1000 Torr - 10^{-6} Torr. About 20 mg of powder sample was pressed onto a high-transmittance, lithographically-etched fine tungsten grid which was mounted on a copper sample holder assembly, attached to a ceramic vacuum feedthrough. A K-type thermocouple was spot-welded to the surface of a thin tantalum plate attached on the W-grid to monitor the sample temperature. The sample temperature was controlled within 298 K – 1100 K via a computer-controlled DC resistive heating system using the voltage feedback from the thermocouple. After having mounted the sample in the IR cell, sample was gradually heated to 373 K in vacuum and kept at that temperature for at least 12 h before the experiments in order to ensure the removal of water from the surface and the sytem was baked out. Before each experiment, the walls of the vacuum system were washed by 2 Torr of NO_2 (g) for 10 min followed by evacuation at the same temperature. Next, in order to obtain a surface that is free of adsorbed NO_x and other adsorbates, the sample was annealed in vacuum by increasing the temperature to 1023 K in a linear fashion at a constant rate of 12 K min^{-1}. After this process, sample was cooled down to 323 K. Before acquisition of each spectral series, a background spectrum of the clean, adsorbate-free sample was obtained in vacuum at 323 K at a residual reactor pressure of nearly 10^{-4} Torr. NO_2 (g) (prepared by reacting NO (g), Air Products, Purity > 99.9% and

O_2 (g) (Linde Gaz, Purity > 99.99%)used in the adsorption experiments was further purified via several freeze-thaw-pump cycles before the experiments. SO_2 (g) was prepared by reacting NO (g) and O_2 (g) (Linde Gaz, Purity > 99.99%).

In the current work, two different IR experiment procedures were carried out. The first experiment procedure was performed to investigate SO_x adsorption and thermal stabilities of SO_x species, and the second experiment procedure was performed in order to compare NO_x uptake of the materials before and after SO_x poisoning:

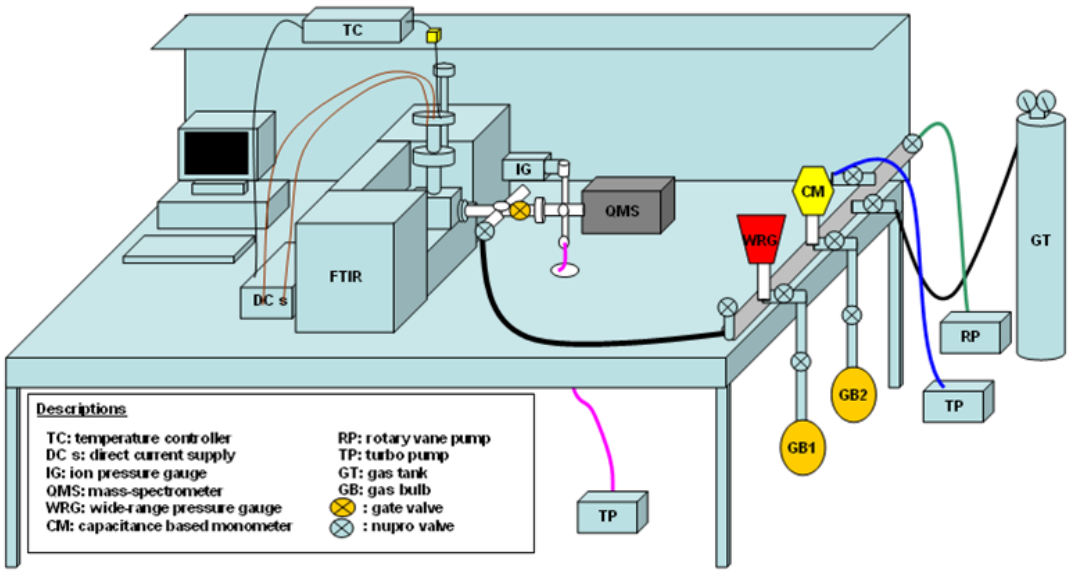

Figure 3. Schematic representation of insitu-FTIR catalytic analysis system coupled to the quadrupole mass spectrometer chamber. Abbreviations used in the scheme are given in the inset above [41].

2.2.1.1 SO_2 (g) + O_2 (g) adsorption experiments

The interaction of SO_2+O_2 with the studied oxide systems was analyzed by in-situ FTIR spectroscopy measurements. The background spectrum of the clean, adsorbate-free sample was obtained at 323 K with a residual reactor pressure < 1 × 10^{-4} Torr. Then, sample was exposed to SO_2 (g) + O_2 (g) (P_{SO2}:P_{O2}= 1:10, P_{Total} = 0.6 Torr) at 323 K for 15 minutes. After 15 minutes, IR spectrum was acquired., Sample was initially heated to 473 K in a linear fashion and at this temperature the sample was allowed to interact with SO_2+O_2 for 30 minutes. Then the sample was cooled to 323 K in the gas mixture, followed by the acquisition of the IR spectrum. In the second step, sample is annealed to 573 K in the gas mixture and the sample was kept at this temperature for 30 minutes in the presence of SO_2 + O_2, followed by cooling of to 323 K and acquisition of the IR spectrum. Then the sample was stepwise heated to 673 K, 773 K, 873 K repeating the procedure described for the first and second steps. After that, IR cell was evacuated and IR spectrum was acquired at 323 K. Next, for observing the thermal stabilities of SO_x species, sample was consequently flashed to different temperatures (473 K, 573 K, 673 K, 773 K, 873 K, 973 K, 1073K and 1173 K) in vacuum respectively, followed by the cooling of the sample to 323 K and the acquisition of sample spectrum.

2.2.1.2 The Effect of Sulfur Poisoning on NO_x Uptake

The NO_x uptake capacity of the studied oxide systems before and after the poisoning was investigated by in-situ FTIR spectroscopy measurements as well. The background spectrum of the clean, adsorbate-free sample was obtained at 323 K with a residual reactor pressure < 1 × 10^{-4} Torr. Then, the sample was exposed to a precisely controlled dose of NO_2 (P_{NO2} = 8.0 Torr) for 10 min at 323 K. After the saturation of the sample, the system was evacuated at room temperature ($P_{reactor}$ < 1 × 10^{-4} Torr) and an IR spectrum of the sample was taken. Then the sample was flashed to 1023 K in a linear fashion to perform TPD and cooled back to 323 K for the next IR spectrum. After that, SO_2 (g) + O_2 (g) (P_{SO2}:P_{O2}= 1:10) (P_{Total} = 0.6 Torr) was introduced over the sample at 323 K and the temperature of the sample was increased to 673 K (473 K) in a linear fashion and sample was allowed to interact with SO_2+O_2

at this temperature for 30 minutes. After cooling to 323 K IR spectrum was obtained (in the presence of SO_2+O_2 gas). Next, the reactor was evacuated and the IR spectrum was acquired again. In order to investigate the NO_x uptake after poisoning, the sample was saturated with NO_2 (P_{NO2} = 8.0 Torr) at 323 K for 10 minutes. Then the IR cell was evacuated, followed by acquiring of IR spectrum. Lastly, the sample was heated to 1173 K in a linear fashion to perform TPD and cooled to 323 K followed by IR analysis.

2.2.2 TPD

In the TPD experiments the samples were heated with a linear ramp of 12 K/min to 1023 K (for NO_x uptake experiments) or 1173 K (for SO_x poisoning experiements). TPD spectra were acquired by using a quadruple mass spectrometer (QMS, Stanford Research Systems, RGA 200), which was directly connected to the vacuum chamber through a pneumatic gate valve. Prior to each TPD experiment, oxidation-resistant thoria coated iridium filament of the mass spectrometer was outgased for 30 min. A powder sample (mass = c.a. 20 mg) was pressed onto a tungsten grid (that allows to heat the sample resistively by passing current through the grid with precisely uniform temperature distribution over all sample surface) which was mounted in the IR/TPD cell. Before TPD experiments the sample surface was activated in the IR cell by dosing 2 Torr of NO_2 over the sample for 10 minutes at 323 K, followed by the evacuation of the sample. Next, the sample was annealed to 1023 K in order to have an adsorbate-free surface. Then, the sample was exposed to a precisely controlled dose of NO_2 (P_{NO2} = 8.0 Torr) for 10 min at 323 K. After the evacuation, TPD experiment was performed while the sample was being heated to 1023 K with a ramp rate of 12 K/min. Analogous experiments were performed with SO_x poisoned samples where the sample was heated to 1173 K. The QMS signals with m/z equal to 18(H_2O), 28(N_2/CO), 30(NO), 34(H_2S), 32(O_2), 44(N_2O/CO_2), 46(NO_2) and 64(SO_2) were monitored during the TPD measurements.

2.2.3 XPS

XPS data were recorded using a SPECS spectrometer with a PHOIBOS 100/150 hemispherical energy analyzer and a monochromatic AlK_{α} X-ray irradiation ($h\nu$ = 1486.74 eV, 400 W). Binding energy scale was preliminarily calibrated via the position of the Au $4f_{7/2}$ (84.0 eV) and Cu $2p_{3/2}$ (932.7 eV) core level signals. Surface atomic concentration ratios of the elements were calculated from the integral intensities of photoelectron peaks corrected by the corresponding atomic sensitivity factors (ASF).

2.2.4 SEM/EDX

SEM and EDX data were performed using a Zeiss EVO40 environmental SEM that is equipped with a LaB_6 electron gun, a vacuum SE detector, an elevated pressure SE detector, a backscattering electron detector (BSD) and a Bruker AXS XFlash 4010 detector. Samples for SEM and EDX analysis were prepared by grinding the samples into fine powder and mechanically dispersing them on an electrically conductive carbon film which was placed on an aluminium sample holder. SEM images were obtained using a vacuum SE detector where electron acceleration voltage of the incident beam was varied within 10-20 kV and the samples were kept typically at $\leq 5 \times 10^{-5}$ Torr inside the SEM. All of the EDX data were collected using an electron acceleration voltage of 20 kV and a working distance of 15 mm. For the EDX elemental mapping studies, at least three independent areas of identical dimensions on the same catalyst sample were investigated in order to assure the reproducibility of the results.

3 RESULTS AND DISCUSSION

3.1 SO_x interaction with Fe promoted Ba/Al_2O_3 catalytic support materials by means of FTIR

Before discussing SO_2+O_2 adsorption on the surfaces of $Fe/Ba/Al_2O_3$ samples at different temperatures, firstly, interaction of SO_2+O_2 with γ-Al_2O_3 should be considered as benchmark material. γ-Al_2O_3 interaction with SO_2 and SO_2+O_2 was intensively investigated previously and these experiments have been also performed in our laboratory previously. Karge et al. [42] investigated SO_2 (g) adsorption on the alumina surface via FTIR. SO_2 was observed to bind to the basic sites on alumina and form adsorbed sulfite (SO_3^{2-}) species. The sulfite species are converted into sulfate (SO_4^{2-}) species upon oxidation. IR bands related to weakly and strongly adsorbed SO_2 species appear after exposure of the alumina surface to SO_2. The adsorption of SO_2 on the basic adsorption sites is followed by a cleavage of an Al-O bond (primarily at OH sites and exposed oxygen atoms, O^{2-}) leading to the formation of chemisorbed SO_3^{2-}, while adsorption at acidic sites (Al^{3+}) forms physisorbed SO_2 species. The oxidation of adsorbed sulfite (SO_3^{2-}) species and SO_2 in oxygen at relatively high temperatures (673-773 K) gives rise to two strong intense bands related to surface sulfate species which are coordinated to the metal cations of the oxide surface through three oxygen atoms [43]. In literature, there are a large number of similar studies one of which showed that SO_2 adsorption on an alumina sample formed surface aluminium sulfate (1318 cm^{-1}) and sulfite (972 cm^{-1}) species [44]. In another study, Saur et al. [45] reported that surface aluminium sulfate is characterised by two features at 1380 cm^{-1} and 1035 cm^{-1}.

In our laboratory, Şentürk et al. [46] studied the SO_2+O_2 adsorption on the γ-Al_2O_3 surface via FTIR. These experiments are represented in Figure 4. SO_2 (g) + O_2 (g) adsorption on γ-Al_2O_3 (Figure 4, *spectrum a*) yields a major broad band at 1068 cm^{-1} and weaker and poorly-defined additional features around 1350, 1250 and 994 cm^{-1}. The signal at 1068 cm^{-1} with a shoulder at 1050 cm^{-1} is due to the presence of

sulfite (SO_3^{2-}) species. The features at 1368, 1170 and 994 cm^{-1} did become more visible as the adsorption temperature increases to 473 K (Figure 4, *spectra b*). Minor features in Figure 3 at 1350 cm^{-1} (ν_{as}, S-O) and the broad band at 1150 cm^{-1} (ν_s, S-O) were assigned to weakly adsorbed molecular SO_2. The ν (S=O) surface sulfate at 1368 cm^{-1} was seen to start growing after heating to 473 K. The band at 1250 cm^{-1} was reported to be related to bidentate sulfate species which transform into bulk $Al_2(SO_4)_3$ (1170 cm^{-1}) as temperature increases.

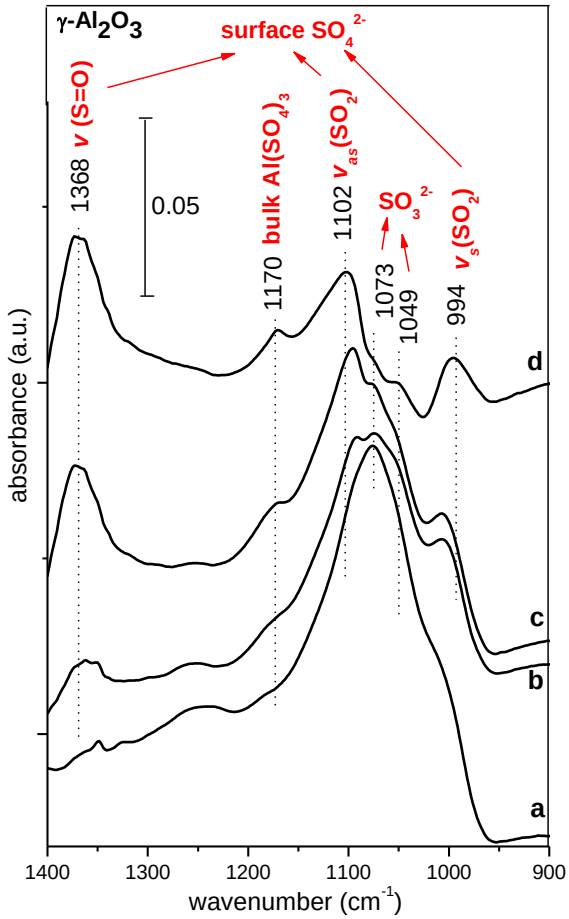

Figure 4. FTIR spectra for SO_2 (g) + O_2 (g) (SO_2:O_2, 0.1:1) co-adsorption on γ-Al_2O_3. **a)** After 1 h exposure to SO_2 (g) + O_2 (g) at 323 K (spectrum was obtained in the presence of the gas mixture), **b)** after flashing the sample in (a) to 473 K in SO_2 + O_2 and cooling to 323 K (spectrum was obtained in the presence of the gas mixture), **c)** after flashing the sample in (b) to 673 K in SO_2 (g) + O_2 (g) and further evacuation at 323 K for 20 min ($P_{reactor} < 1\times10^{-4}$ Torr) , **d)** after flashing the sample in (c) to 673K in vacuum ($P_{reactor} < 1\times10^{-4}$ Torr) and cooling to 323 K [46].

After increasing the temperature to 673 K and evacuating at 323 K (Figure 4, *spectra c*), the weakly adsorbed molecular SO_2 species at 1350 and 1150 cm^{-1} were reported to be oxidized to SO_x species, which are evident with the bands at 1368, 1170 and 994 cm^{-1}. The features at 1368 cm^{-1} (ν (S=O)), 1097 cm^{-1} (ν_{as} (SO_2)) and 994 cm^{-1} (ν_s (SO_2)) appear as the dominant features after annealing at 673 K in vacuum (Figure 4, *spectra d*). The smaller bands observed at 1068 and 1050 cm^{-1} in Figure 4 (spectrum *g*) ,which were attributed to tri-coordinated sulfite species, were observed to become less pronounced in the presence of sulfates. The minor feature at 1170 cm^{-1}, which was still being visible after flashing the sample to 473 K in vacuum, was announced to indicate the presence of bulk $Al_2(SO_4)_3$.

In the light of these results it was concluded that sulfites and sulfates are initially formed on the surface at the beginning of the SO_2 adsorption and at elevated temperatures, these species are successively converted into relatively stable surface sulfates as well as bulk $Al_2(SO_4)_3$.

The other benchmark samples, 5Fe/Al, 10Fe/Al, 8Ba/Al and 20Ba/Al, were also subjected to SO_2+O_2 adsorption experiment.

SO_2+O_2 exposure on 5Fe/Al at 323 K (Figure 5, spectrum *a*) reveals a broad band at 1000-1100 cm^{-1} and a minor feature at 1350 cm^{-1}. The broad feature between 1000-1100 cm^{-1} can be attributed to the overlapping peaks of sulfate (SO_4^{2-}) and sulfites (SO_3^{2-}) species on Fe oxide and Al oxide surfaces. Unfortunately this broad feature is convoluted and overlapping peaks cannot be separated. The feature at 1020 cm^{-1} may be attributed to the presence of bidentate sulfates on Fe oxide. Yamaguchi et al. reported that the formation of sulfates on Fe oxide which is evident with the IR feature at 1020 cm^{-1} [47]. Fu et al. [37] studied the oxidation of SO_2 on α-Fe_2O_3 via FTIR and they observed a band at 1042 cm^{-1} which they assigned as SO_2 bound to the surface through two oxygen atoms resulting in the formation of the bidentate-surface complexes. Moreover, they reported the formation of bidentate sulfato-metal surface complexes on the surface of Fe_3O_4 upon oxidation, which is evident with the IR bands between 1000-1300 cm^{-1}. These former investigations are in good agreement with our FTIR results. After flashing the sample to 473 K in SO_2 (Figure 5, spectrum *b*), the feature at 1378 cm^{-1} becomes more visible. According to Saur et al. [45] this feature indicates the presence of sulfate where three oxygens of sulfate specie are bounded to Al^{3+} sites. In addition, Yamaguchi et al. [47] attributed the

1380 cm^{-1} feature to the bidentate or chelating sulfates on Fe_2O_3. Therefore in the current work this feature is assigned to the overlapping band of surface sulfates on Al and/or Fe oxides. This feature at 1378 cm^{-1} keeps growing in intensity until the temperature of the sample is inceased to 673 K upon heating in SO_2+O_2. In addition a new broad band between 1000-1100 cm^{-1} appears at that temperature (Figure 5, spectrum *d*). The additional signal at 1095 cm^{-1} which becomes also visible corresponds to the ν_1 mode of surface sulfates on Al_2O_3 [43]. The 1073 cm^{-1} feature indicates the presence of sulfite (SO_3^{2-}) [48]. After the sample is annealed to 773 K in SO_2+O_2 (Figure 5, spectrum *e*), a new weak but distinguishable band rises at 1230 cm^{-1}, which is attributed to the sulfates on Fe oxide. This is consistent with a former study elucidating that the peak 1230 cm^{-1} arises together with the feature at 1042 cm^{-1} [37]. In addition, the signal at 1020 cm^{-1} (sulfates on Fe oxide) becomes distinguishable after the temperature of the sample is increased to 773 K. At 873 K in SO_2+O_2 (Figure 5, spectrum *f*), a new shoulder appears at ~ 1390 cm^{-1}, also the feature at 1230 cm^{-1} (sulfates on Fe oxide) becomes more announced. These changes can be ascribed to the subsequent sulfation of the surface where alumina surface is initially sulfated, followed by the sulfation of Fe sites at T > 873 K.

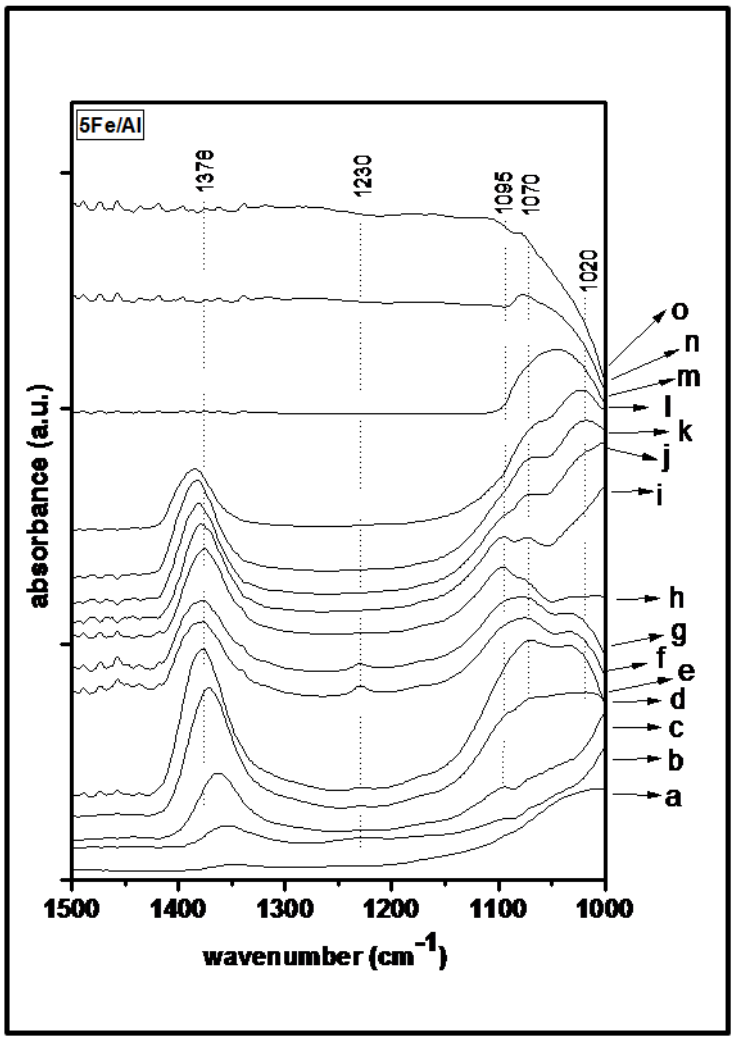

Figure 5. FTIR spectra for 0.6 Torr SO_2+O_2 (1:10) adsorption on 5Fe/Al. **a)** After 15 min exposure to SO_2+O_2 at 323 K, **b)** after flashing the (a) sample to 473 K and cooling to 323 K, **c)** after flashing the (b) sample to 573 K and cooling to 323 K, **d)** after flashing the (c) sample to 673K and cooling to 323 K, **e)** after flashing the (d) sample to 773 K and cooling to 323 K, **f)** after flashing the (e) sample to 873 K and cooling to 323 K, **g)** after evacuation of the reactor ($P_{reactor} < 1\times10^{-4}$ Torr), **h)** after flashing the (g) sample to 473 K and cooling to 323 K, **i)** after flashing the (h) sample to 573 K and cooling to 323 K, **j)** after flashing the (i) sample to 673 K and cooling to 323 K, **k)** after flashing the (j) sample to 773 K and cooling to 323 K, **l)** after flashing the (k) sample in to 873 K and cooling to 323 K, **m)** after flashing the (l) sample to 973 K and cooling to 323 K, **n)** after flashing the (m) sample to 1073 K and cooling to 323 K, **o)** after flashing the (n) sample to 1173 K and cooling to 323 K. (spectra **a-f** were taken in the gas mixture; spectra **g-o** were taken in vacuum.)

After evacuation of the gas mixture from the reactor followed by annealing of the sample in vacuum to 473 K (Figure 5, spectrum *h*) it is evident that the features related to sulfates on Fe (1020 and 1230 cm^{-1}) and the shoulder at 1390 cm^{-1} disappear, which suggest that sulfates on Fe oxide start to decompose even at 473 K. After flashing the sample to 573 K in vacuum (Figure 5, spectrum *i*), the feature (1070 cm^{-1}) corresponding to sulfite (SO_3^{2-}) becomes visible again indicating the partial decomposition of sulfates (on Fe oxide) to sulfites. After heating of the sample to 873 K in vacuum (Figure 5, spectrum *l*), intensity of sulfate features at 1378 cm^{-1} and 1095 cm^{-1} are getting smaller pointing out that surface sulfates on Al oxide starts to decompose. As the sample is flashed to 973 K, the peak at 1378 cm^{-1} completely vanishes indicating the decomposition of most of the surface sulfate species. The minor sulfite feature at 1070 cm^{-1} which is left after heating the sample to 1173 K in vacuum (Figure 5, spectrum *o*) when most of the sulfates are decomposed points to the higher thermal stability of the sulfites on alumina.

SO_2+O_2 adsorption on 5Fe/Al sample (Figure 5) shows that at the beginning of SO_2 exposure, sulfites and sulfates on alumina start to form. As the temperature is increased to 773 K in SO_2, sulfites are further oxidized to sulfates and sulfates on Fe sites are also formed. At 873 K in SO_2+O_2, sulfate formation on the alumina domains reaches saturation while sulfation of the Fe sites continues. After evacuation of the gas followed by flashing the sample to 473 K, sulfates on Fe oxide decompose completely, and after further heating to 973 K sulfates on alumina decompose and also form sulfites. These results show that it is more favorable and easier for alumina to form sulfate, in comparison to Fe oxide, and sulfates of alumina are more stable than the ones on Fe.

SO_2+O_2 exposure on 10Fe/Al sample (Figure 6) at 323 K leads to the formation of similar species as in the case of 5Fe/Al. The minor feature appearing at 1037 cm^{-1} after the sample is heated to 473 K (Figure 6, spectrum *b*) may be assigned to the surface sulfate species. The reason why this band was not well distinguishable in the case of 5Fe/Al sample may be arising from the increased quantity of sulfates that are formed when Fe loading is increased to 10wt%. The most pronounced difference in the adsorption of SO_2 on 5Fe/Al and 10Fe/Al is the difference in decomposition temperature of sulfates on alumina domains.

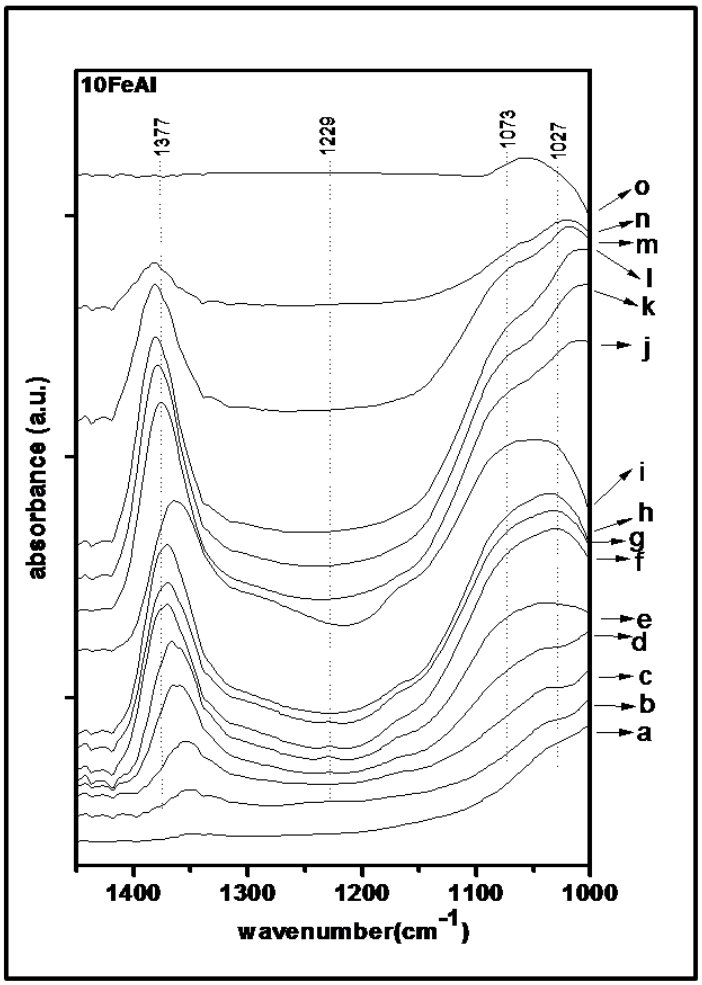

Figure 6. FTIR spectra for 0.6 Torr SO_2+O_2 (1:10) adsorption on 10Fe/Al. **a)** After 15 min exposure to SO_2+O_2 at 323 K, **b)** after flashing the (a) sample to 473 K and cooling to 323 K, **c)** after flashing the (b) sample to 573 K and cooling to 323 K, **d)** after flashing the (c) sample to 673K and cooling to 323 K, **e)** after flashing the (d) sample to 773 K and cooling to 323 K, **f)** after flashing the (e) sample to 873 K and cooling to 323 K, **g)** after evacuation of the reactor ($P_{reactor} < 1\times10^{-4}$ Torr), **h)** after flashing the (g) sample to 473 K and cooling to 323 K, **i)** after flashing the (h) sample to 573 K and cooling to 323 K, **j)** after flashing the (i) sample to 673 K and cooling to 323 K, **k)** after flashing the (j) sample to 773 K and cooling to 323 K, **l)** after flashing the (k) sample in to 873 K and cooling to 323 K, **m)** after flashing the (l) sample to 973 K and cooling to 323 K, **n)** after flashing the (m) sample to 1073 K and cooling to 323 K, **o)** after flashing the (n) sample to 1173 K and cooling to 323 K. (spectra **a-f** were taken in the gas mixture; spectra **g-o** were taken in vacuum.)

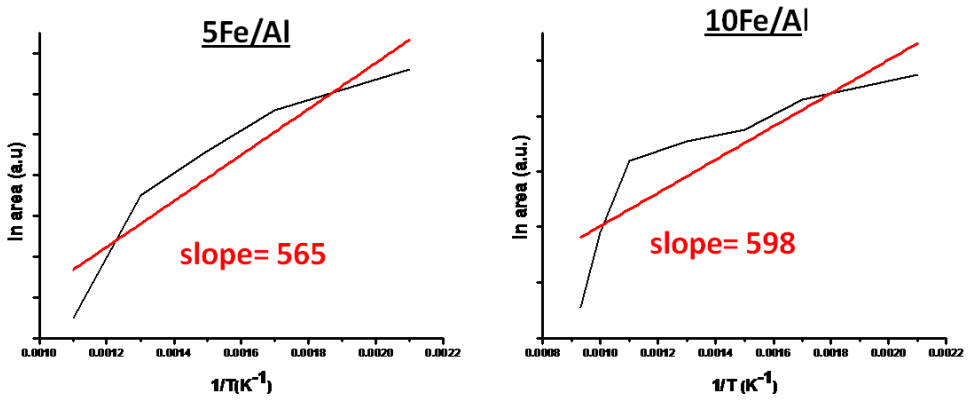

Figure 7. 1/T vs. natural logarithm of the integrated FTIR peak areas of the feature centered at 1380 cm-1 for **a)** 5Fe/Al and **b)** 10Fe/Al.

The sulfates on alumina domains of 5Fe/Al sample decompose after heating the sample to 973 K (Figure 6, spectrum *o*), whereas decomposition of sulfates on γ-Al_2O_3 occurs after annealing the sample to 1173 K on 10Fe/Al. This may be due to the fact that higher loading of Fe covers most of the Al surface and provides a diffusion barrier for the SO_x encapsulated in the underlying alumina domains.

The fact that the feature at 1380 cm^{-1} belongs to the same species on the surface of both 5Fe/Al and 10Fe/Al samples can be demonstrated with the curve (Figure 7) representing 1/T vs. natural logarithm of the integrated FTIR peak area. The slopes of the curves (based on Arrhenius plot) can be related to the activation energies for decomposition of the corresponding species. Since the slopes are comparable, the 1380 cm^{-1} band is attributed to the same species on the surface of 5Fe/Al and 10Fe/Al samples.

It is well known that the NO_x storage component NSR catalysts react with SO_2 in oxidizing conditions and SO_2 can be readily oxidized on the NSR catalyst forming $BaSO_4$ which deactivates the catalyst [49, 50]. The addition of Fe into the binary 8(20)BaO/Al_2O_3 systems is a promising approach to this problem [49, 50]. This part of the current study deals with the fundamental understanding of the surface chemistry upon SO_2+O_2 exposure on the Ba containing ternary $Fe/Ba/Al_2O_3$ oxide systems via FTIR.

Before investigating the sulfation process occurring on the complex $Fe/Ba/Al_2O_3$ oxide system, the IR-spectra of the SO_2+O_2 adsorption on the 8Ba/Al and 20Ba/Al binary oxide system were studied.

During the adsorption of SO_2 at 323 K (Figure 8, spectrum *a*), 8Ba/Al sample reveals a broad band between 1000-1100 cm^{-1} indicating the presence of overlapping of different kinds of sulfites (and sulfates) on the surface. In this region of the spectra two lines may be discernible. These are the minor peaks at 1060 and 1118 cm^{-1} which are attributed to the surface sulfates on BaO. When the sample temperature is increased to 473 K (Figure 8, spectrum *b*), an additional band at 1100 cm^{-1} becomes apparent. This band is characteristic of the S-O stretching vibrations of bidentate sulfates located on the surface of BaO [51]. After flashing the sample to 573 K (Figure 6, spectrum *c*), the additional minor features at 1162 cm^{-1}, 1245 cm^{-1} , and 1040 cm^{-1} rise, which indicates the presence of bulk barium sulfates [51, 52]. This leads the statement that at 573 K, both surface and bulk sulfates exist on BaO domains. Interaction of 8Ba/Al storage component with SO_2 at 673 K (Figure 8, spectrum *d*) reveals two additional bands at 1350 cm^{-1} and 1312 cm^{-1}. Moreover, the intensities of the bands at 1040 cm^{-1}, 1162 cm^{-1} and 1245 cm^{-1} are increasing. The minor feature at 1350 cm^{-1} corresponds to the ν(S=O) vibration and is attributed to the tri-coordinated sulfate species on the Al_2O_3 support [50]. In addition to the tri-coordinated sulfates, the presence of bridging sulfates on Al is clear with the feature at 1312 cm^{-1} [43, 53, 54]. The growing peaks corresponding to the bulk barium sulfates point to the transformation and/or migration of surface sulfates to bulk sulfates at 673 K. After the temperature of the sample is increased to 873 K (Figure 8, spectrum *f*), the shape of the spectrum shows a minor change in the region belonging to sulfates on Al_2O_3 support. The overlap of different types of sulfate species on Al gives a broad band between 1312-1380 cm^{-1}. The sulfates on Al form

at higher temperature than the ones on Ba, which indicates that formation of $BaSO_4$ is more favourable thermodynamically than the formation of $Al_2(SO_4)_3$.

Table 2 represents the Gibbs free energies of formation of $FeSO_4$ (s), $BaSO_4$ (s) and $Al_2(SO_4)_3$ (s). Our results demonstrating that formation of $BaSO_4$ is more favourable than the formation of $Al_2(SO_4)_3$ are not consistent with the results shown in Table 2. This is due to the significant differences in the chemical environment and size of the species.

Table 2. Gibbs free energies of formation of $FeSO_4$, $BaSO_4$, $Al_2(SO_4)_3$ [55].

	$FeSO_4$ (s)	**$BaSO_4$ (s)**	**$Al_2(SO_4)_3$ (s)**
Gibbs Free Energy (kJ/mol)	-825. 1	-1362.2	-3506.6

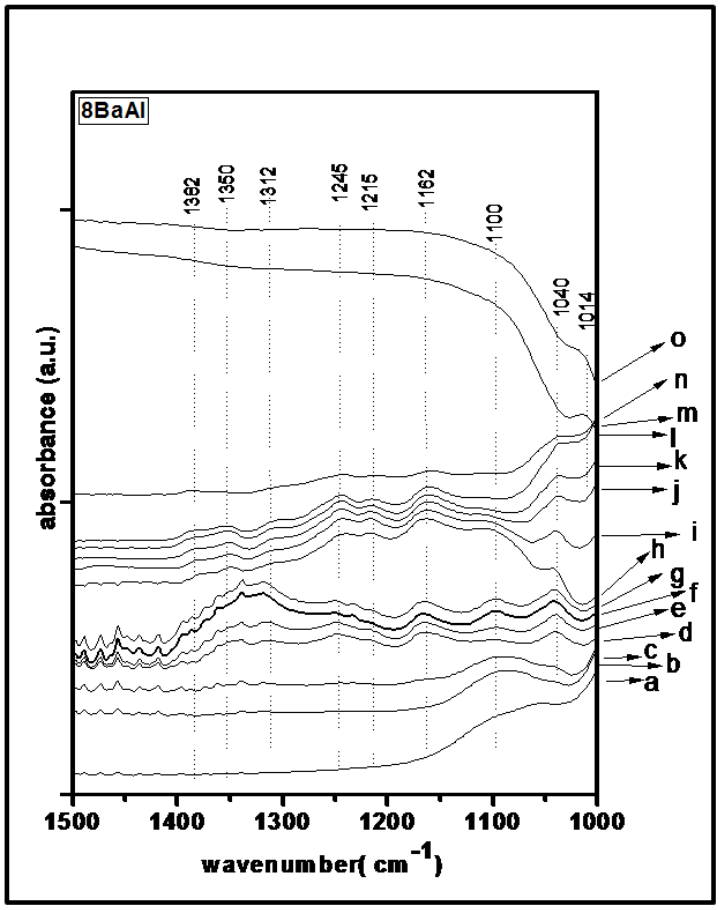

Figure 8. FTIR spectra for 0.6 Torr SO_2+O_2 (1:10) adsorption on 8Ba/Al. **a)** After 15 min exposure to SO_2+O_2 at 323 K, **b)** after flashing the (a) sample to 473 K and cooling to 323 K, **c)** after flashing the (b) sample to 573 K and cooling to 323 K, **d)** after flashing the (c) sample to 673K and cooling to 323 K, **e)** after flashing the (d) sample to 773 K and cooling to 323 K, **f)** after flashing the (e) sample to 873 K and cooling to 323 K, **g)** after evacuation of the reactor ($P_{reactor} < 1\times10^{-4}$ Torr), **h)** after flashing the (g) sample to 473 K and cooling to 323 K, **i)** after flashing the (h) sample to 573 K and cooling to 323 K, **j)** after flashing the (i) sample to 673 K and cooling to 323 K, **k)** after flashing the (j) sample to 773 K and cooling to 323 K, **l)** after flashing the (k) sample in to 873 K and cooling to 323 K, **m)** after flashing the (l) sample to 973 K and cooling to 323 K, **n)** after flashing the (m) sample to 1073 K and cooling to 323 K, **o)** after flashing the (n) sample to 1173 K and cooling to 323 K. (spectra **a-f** were taken in the gas mixture; spectra **g-o** were taken in vacuum.)

After evacuation of the gas followed with the heating of the sample to 473 K in vacuum (Figure 8, spectrum *h*), the most pronounced change in spectrum is the decrease in the intensity of the broad feature (1312-1380 cm^{-1}) corresponding to surface sulfates on Al. Moreover, the band at 1100 cm^{-1} which is the characteristic stretching vibration of bidentate surface on Ba shows a dramatic decline in intensity. With the further heating of the sample until 873 K (Figure 8, spectrum *l*) surface sulfates on Al bands continues to diminish. After flashing the sample to 973 K (Figure 8, spectrum *m*), it becomes hard to detect both bulk $BaSO_4$ and surface aluminium sulfates and finally most of the sulfates decompose into sulfites which are evident with feature at 1014 cm^{-1}.

For the interaction of 8Ba/Al storage material with SO_2 in oxidizing conditions, it can be proposed that at lower temperatures (273 K) surface sulfites and sulfates are formed. With further heating in SO_x, sulfites turn to sulfates by means of oxidation and surface sulfates transform to bulk sulfates. The formation of $Al_2(SO_4)_3$ is observed to take place at higher temperature than the formation of $BaSO_4$. At higher temperature (T > 973 K) (heating in vacuum) decomposition of surface aluminum sulfates followed by the decomposition of bulk aluminum sulfates and barium sulfates.

SO_2+O_2 adsorption was also performed on another benchmark sample; 20Ba/Al (Figure 9). Interaction of the sample with SO_x at 273 K (Figure 9, spectrum *a*) results in the formation of similar SO_x species observed on the surface of 8Ba/Al. The broad region between 1000-1100 cm^{-1} indicates the presence of sulfites (and surface sulfates). After the sample temperature is increased to 573 K (Figure 9, spectrum *c*), bulk barium sulfates becomes apparent with the features at 1045 cm^{-1}, 1160 cm^{-1} and 1240 cm^{-1}. The bulk barium sulfate bands continue to grow in intensity until the sample is heated to 773 K (Figure 9, spectrum *e*). After the sample is flashed to 873 K in SO_x (Figure 9, spectrum *f*), an additional broad band corresponding to alumina sulfates is appeared. The formation of sulfates on Al_2O_3 support is not as visible as on the surface of 8Ba/Al in comparison to these types of sulfates on the surface of 20Ba/Al. First BaO domains interact with SO_2 and then Al_2O_3 reacts with SO_2 to form sulfates. Since 20wt%BaO covers a larger fraction of the Al_2O_3 surface in comparison to 8wt%BaO, sulfate formation on the alumina sites is suppressed on the surface of 20Ba/Al. After the evacuation of the gas and further

heating of the sample to 473 K in vacuum (Figure 9, spectrum *h*), the broad peak at 1350 cm^{-1} disappears which points the decomposition of alumina sulfates. There is no change in the line shape of the spectrum when the sample is heated in vacuum up to 973 K. After 973 K (Figure 9, spectrum *m*), a minor change can be seen in the intensity of the bands at 1240 cm^{-1} and 1160 cm^{-1} showing the beginning of the bulk barium sulfate decomposition. After the sample is flashed to 1073 K (Figure 9, spectrum *n*) all features are significantly diminished. The further heating of the sample to 1173 K (Figure 9, spectrum *o)* shows a small quantity of sulfates and sulfites on the surface of the 20Ba/Al sample.

The 8Ba/Al and 20Ba/Al samples, on which SO_2+O_2 adsorption experiments were performed, shows some differences in interaction with SO_x. Firstly, more bulk barium sulfate is formed on the surface of 20Ba/Al sample, obviously due to the high content of BaO domains. Then, since formation of alumina sulfate starts after the formation of barium sulfate, the bands belonging to alumina sulfate become visible after heating of the sample in SO_x to higher temperature in case 20Ba/Al sample. Furthermore, bulk alumina and barium sulfates have comparable thermal stabilities and desorb at relatively similar temperatures.

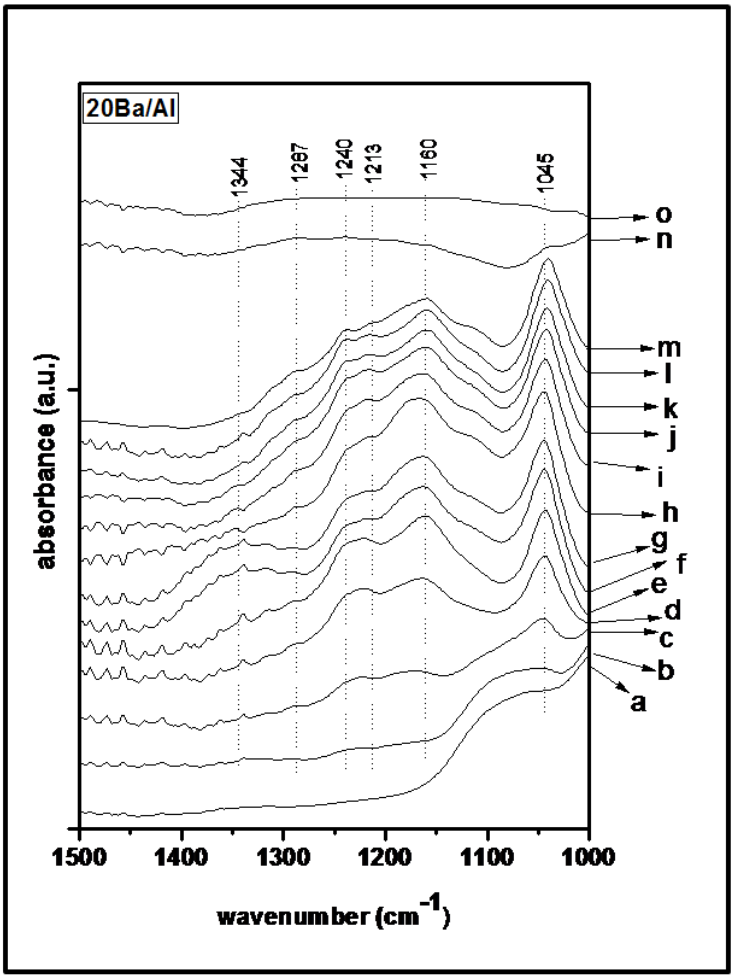

Figure 9. FTIR spectra for 0.6 Torr SO_2+O_2 (1:10) adsorption on 20Ba/Al. **a)** After 15 min exposure to SO_2+O_2 at 323 K, **b)** after flashing the (a) sample to 473 K and cooling to 323 K, **c)** after flashing the (b) sample to 573 K and cooling to 323 K, **d)** after flashing the (c) sample to 673K and cooling to 323 K, **e)** after flashing the (d) sample to 773 K and cooling to 323 K, **f)** after flashing the (e) sample to 873 K and cooling to 323 K, **g)** after evacuation of the reactor ($P_{reactor} < 1\times10^{-4}$ Torr), **h)** after flashing the (g) sample to 473 K and cooling to 323 K, **i)** after flashing the (h) sample to 573 K and cooling to 323 K, **j)** after flashing the (i) sample to 673 K and cooling to 323 K, **k)** after flashing the (j) sample to 773 K and cooling to 323 K, **l)** after flashing the (k) sample in to 873 K and cooling to 323 K, **m)** after flashing the (l) sample to 973 K and cooling to 323 K, **n)** after flashing the (m) sample to 1073 K and cooling to 323 K, **o)** after flashing the (n) sample to 1173 K and cooling to 323 K. (spectra **a-f** were taken in the gas mixture; spectra **g-o** were taken in vacuum.)

In order to illustrate the influence of FeO_x on the Ba/Al systems, sulfur poisoning experiments were performed for the 5(10)Fe/8(20)Ba/Al samples. SO_x adsorption at 323 K on the surface of 5Fe/8Ba/Al sample (Figure 10, spectrum *a*) reveals a broad band between 1000-1150 cm^{-1}. This broad feature is attributed to the presence of sulfites on Al_2O_3, BaO and/or FeO_x domains. With the heating of the sample to 573 K (Figure 10, spectrum *c*) in SO_x, the signals at 1040 cm^{-1} and 1360 cm^{-1} corresponding to bulk barium sulfates and surface sulfates on Al_2O_3 become distinctive. Moreover, there are three minor features at 1157 cm^{-1}, 1231 cm^{-1} and 1246 cm^{-1}. The bands at 1157 cm^{-1} and 1246 cm^{-1} support the formation of bulk barium sulfates with the feature at 1040 cm^{-1}. The presence of 1231 cm^{-1} peak indicates the formation of sulfates on FeO_x domains. After further heating of the sample in SO_x to 673 K (Figure 10, spectrum *d*), the intensities of all the features grow significantly. After annealing of the sample to 873 K in SO_x (Figure 10, spectrum *f*), the sulfates on FeO_x domains become more apparent at 1231 cm^{-1}, in addition the band corresponding to surface alumina sulfates (1360 cm^{-1}) gets reduced in intensity. After the evacuation followed by the heating of the sample to 437 K in vacuum (Figure 10, spectrum *h*), disappearance of the peak at 1231 cm^{-1} is the most pronounced change in the line shape of the spectrum, which points out that iron sulfates start decompose after 437 K. It is also clear that the band at 1360 cm^{-1} corresponding to alumina sulfates continue to decrease in intensity. The signals which belong to bulk barium sulfates are not changed until the temperature of the sample is increased to 973 K in vacuum. After the sample is flashed to 973 K in vacuum (Figure 10, spectrum *m*), the broad feature at 1360 cm-1 disappears indicating complete decomposition of the surface alumina sulfates. Presumably, decomposition of alumina sulfates results in the formation of sulfites which give two signals: a minor band at 1114 cm^{-1} and a broad band at around 1068 cm^{-1}. Heating of the sample to 1173 K in vacuum (Figure 10, spectrum *o*) results in almost straight spectrum line pointing that most of the sulfites and sulfates are decomposed.

Considering these results reveals that, addition of 5%wt of Fe to 8Ba/Al results in significant changes. Formation of sulfates on alumina domains is observed to start at lower temperatures such as 573 K; while on 8Ba/Al sample aluminium sulfates become apparent above 673 K. Moreover, aluminium sulfates formation is more pronounced for 5Fe/8Ba/Al in comparison to aluminium sulfates on the surface

of 8Ba/Al sample. It is interesting that decomposition of surface aluminium sulfates and Fe sulfates occur at lower temperature (973 K) for 5Fe/8Ba/Al. These observations are in good agreement with the study stating that iron oxide facilitates the deposition of sulfur [56]. Furthermore some highly stable sulfite/sulfate species still exist on the surface even after annealing at 1173 K.

When SO_x was exposed to 10Fe/8Ba/Al (Figure 11) IR spectrum looks very similar to that of 5Fe/8Ba/Al. The adsorption of SO_x on the 10Fe/8Ba/Al sample at 323 K (Figure 11, spectrum *a*) reveals a complex broad peak in 1000-1150 cm^{-1} region which is attributed to the overlapping bands of sulfites on Al_2O_3 and BaO domains. With increasing temperature of SO_x treatment, the bands at 1040 cm^{-1}, 1157 cm^{-1}, 1224 cm^{-1}, 1238 cm^{-1} and 1360 cm^{-1} becomes distinctive (Figure 11, spectrum *c*). As mentioned previously, these are the characteristic features of bulk barium sulfates (1040, 1157, 1238 cm^{-1}), iron sulfates (1224 cm^{-1}), and aluminium sulfates (1360 cm^{-1}). With increasing temperature, the intensities of the features corresponding to bulk barium sulfate and surface Al sulfates grow until the temperature of the sample is increased to 773 K (Figure 11, spectrum *e*). After heating the sample to 873 K (Figure 11, spectrum *f*), the intensity of the sulfate aluminium feature is slightly decreased.. There are no significant changes until the temperature of the sample is increased to 973 K in vacuum. After 973 K (Figure 11, spectrum *m*), the signal at 1360 cm^{-1} disappears, pointing out that aluminium sulfates totally decompose at that temperature. After heating of the sample to 1073 K (Figure 11, spectrum *n*), all Al sulfates are decomposed and only some bulk and surface Ba sulfates are present, which are evident with a broad band centered at 1157 cm^{-1}. Further heating of the sample to 1173 K in vacuum (Figure 11, spectrum *o*) reveals almost no SO_x bands indicating that Ba sulfates are also decomposed.

For 8wt%Ba samples, increasing Fe content results in the formation of much more SO_x species on the alumina support and FeO_x domains. Fe is observed to help the accumulation of SO_x on Al_2O_3 support. However, it also promotes the decomposition of aluminium sulfates which occurs at lower temperatures in comparison to the sample without Fe (i.e. 8Ba/Al). Iron sulfate formation continues even after all BaO domains turn into barium sulfates, but they are not as stable as barium sulfates.

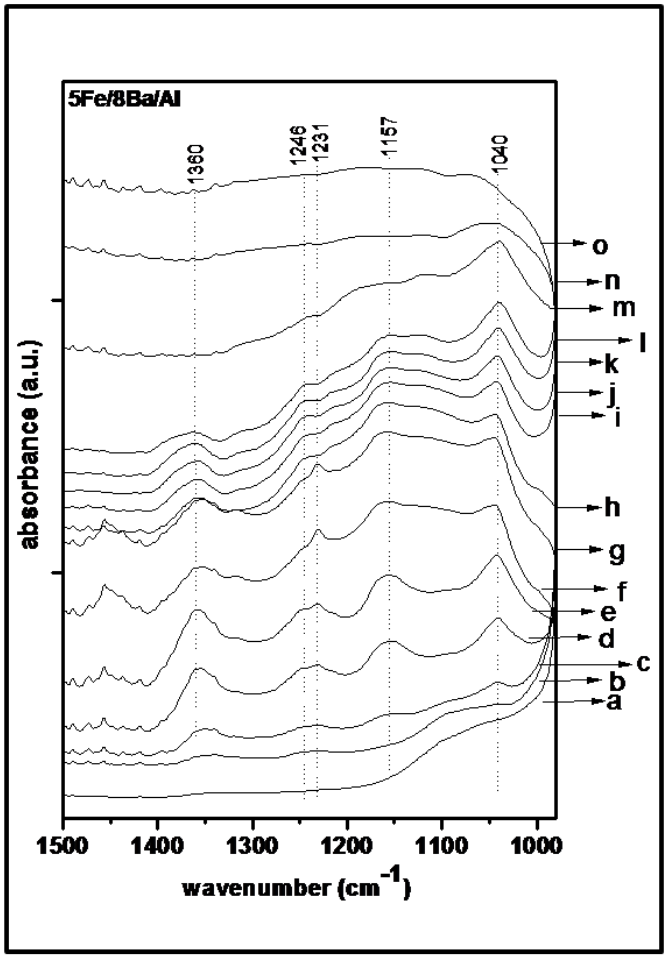

Figure 10. FTIR spectra for 0.6 Torr SO_2+O_2 (1:10) adsorption on 5Fe/8Ba/Al. **a)** After 15 min exposure to SO_2+O_2 at 323 K, **b)** after flashing the (a) sample to 473 K and cooling to 323 K, **c)** after flashing the (b) sample to 573 K and cooling to 323 K, **d)** after flashing the (c) sample to 673K and cooling to 323 K, **e)** after flashing the (d) sample to 773 K and cooling to 323 K, **f)** after flashing the (e) sample to 873 K and cooling to 323 K, **g)** after evacuation of the reactor ($P_{reactor} < 1\times10^{-4}$ Torr), **h)** after flashing the (g) sample to 473 K and cooling to 323 K, **i)** after flashing the (h) sample to 573 K and cooling to 323 K, **j)** after flashing the (i) sample to 673 K and cooling to 323 K, **k)** after flashing the (j) sample to 773 K and cooling to 323 K, **l)** after flashing the (k) sample in to 873 K and cooling to 323 K, **m)** after flashing the (l) sample to 973 K and cooling to 323 K, **n)** after flashing the (m) sample to 1073 K and cooling to 323 K, **o)** after flashing the (n) sample to 1173 K and cooling to 323 K. (spectra **a-f** were taken in the gas mixture; spectra g-o were taken in vacuum.)

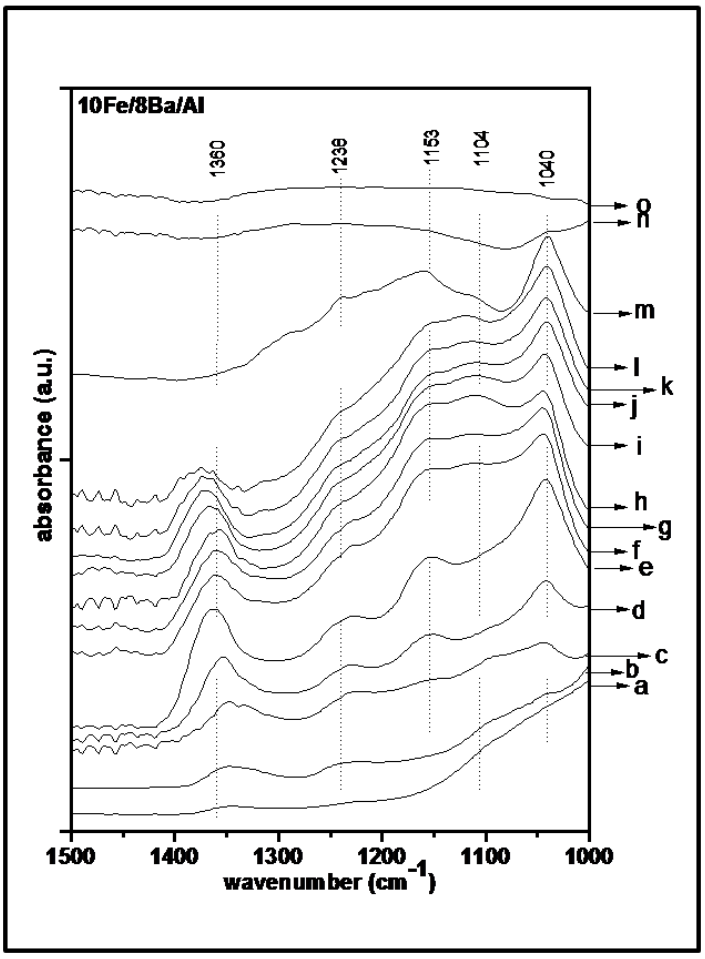

Figure 11. FTIR spectra for 0.6 Torr SO_2+O_2 (1:10) adsorption on 10Fe/8Ba/Al. **a)** After 15 min exposure to SO_2+O_2 at 323 K, **b)** after flashing the (a) sample to 473 K and cooling to 323 K, **c)** after flashing the (b) sample to 573 K and cooling to 323 K, **d)** after flashing the (c) sample to 673K and cooling to 323 K, **e)** after flashing the (d) sample to 773 K and cooling to 323 K, **f)** after flashing the (e) sample to 873 K and cooling to 323 K, **g)** after evacuation of the reactor ($P_{reactor} < 1\times10^{-4}$ Torr), **h)** after flashing the (g) sample to 473 K and cooling to 323 K, **i)** after flashing the (h) sample to 573 K and cooling to 323 K, **j)** after flashing the (i) sample to 673 K and cooling to 323 K, **k)** after flashing the (j) sample to 773 K and cooling to 323 K, **l)** after flashing the (k) sample in to 873 K and cooling to 323 K, **m)** after flashing the (l) sample to 973 K and cooling to 323 K, **n)** after flashing the (m) sample to 1073 K and cooling to 323 K, **o)** after flashing the (n) sample to 1173 K and cooling to 323 K. (spectra **a-f** were taken in the gas mixture; spectra **g-o** were taken in vacuum.)

SO_x exposure on the 5Fe/20Ba/Al sample at 323 K (Figure 12, spectrum *a*) results in the formation of similar species to that formed on the surface of 20Ba/Al. The broad band between 1000-1150 cm^{-1} without distinguishable peak at ~ 1380 cm^{-1} indicates the presence of sulfites on BaO and Al_2O_3 domains. After the sample temperature is increased to 573 K in SO_x (Figure 12, spectrum *c*), sulfites are oxidized forming surface and bulk Ba sulfates which are evident with a new additional peak at 1040 cm^{-1} and with minor features at 1157 cm^{-1}, 1234 cm^{-1}. The 1040 and 1157 cm^{-1} peaks are attributed to bulk barium sulfates and 1234 cm^{-1} peak is attributed to iron sulfates which continue to grow with increasing temperature (in the precence of SO_x gas mixture) until the sample is annealed to 773 K (Figure 12, spectrum *e*). After heating of the sample to 873 K (Figure 12, spectrum *f*), the spectrum reveals two additional signals at 1182 cm^{-1} and 1113 cm^{-1}. The band at 1182 cm^{-1} is attributed to either adsorbed SO_2 [57] or bulk aluminium sulfate [58], and the feature at 1113 cm^{-1} is assigned as surface aluminium sulfates [59]. After evacuation of the gas followed by increasing the temperature to 473 K in vacuum (Figure 12, spectrum *h*), overlapping band of sulfates on Al_2O_3 and FeO_x centered at 1355 cm^{-1} and the minor feature at 1234 cm^{-1} disappear. The line shape of the spectrum does not show a significant change until the sample is flashed to 973 K in vacuum. After heating of the sample to 973 K (Figure 12, spectrum *m*), the bands corresponding to the bulk barium sulfates (1157 cm^{-1}) disappears indicating that decomposition of barium sulfates start after 973 K on the 5Fe/20Ba/Al sample. Annealing of the sample to 1073 K in vacuum (Figure 12, spectrum *n*) results in the decomposition of bulk aluminium sulfates and the barium sulfates almost completely. In addition there is no band corresponding to the sulfites on the surface after heating to 1073 K.

The iron added storage material (5Fe/20Ba/Al) shows important differences compared to the sample which does not contain iron (20Ba/Al). Firstly, formation of the sulfates on Al_2O_3 starts at lower temperature on the surface of 5Fe/20Ba/Al and Fe can be said to increase sulfur uptake ability of Al_2O_3 support. The other significant change is the formation of highly stable bulk aluminium sulfates. Decomposition of bulk barium sulfates also occur at lower temperature than it does on the surface of 20Ba/Al.

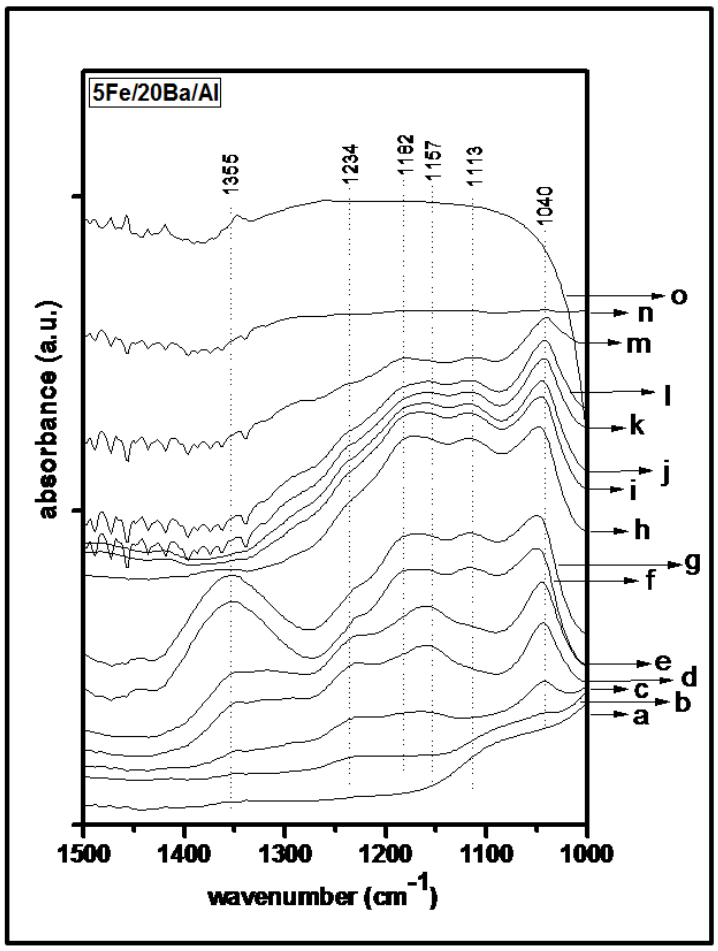

Figure 12. FTIR spectra for 0.6 Torr SO_2+O_2 (1:10) adsorption on 5Fe/20Ba/Al. **a)** After 15 min exposure to SO_2+O_2 at 323 K, **b)** after flashing the (a) sample to 473 K and cooling to 323 K, **c)** after flashing the (b) sample to 573 K and cooling to 323 K, **d)** after flashing the (c) sample to 673K and cooling to 323 K, **e)** after flashing the (d) sample to 773 K and cooling to 323 K, **f)** after flashing the (e) sample to 873 K and cooling to 323 K, **g)** after evacuation of the reactor ($P_{reactor} < 1\times10^{-4}$ Torr), **h)** after flashing the (g) sample to 473 K and cooling to 323 K, **i)** after flashing the (h) sample to 573 K and cooling to 323 K, **j)** after flashing the (i) sample to 673 K and cooling to 323 K, **k)** after flashing the (j) sample to 773 K and cooling to 323 K, **l)** after flashing the (k) sample in to 873 K and cooling to 323 K, **m)** after flashing the (l) sample to 973 K and cooling to 323 K, **n)** after flashing the (m) sample to 1073 K and cooling to 323 K, **o)** after flashing the (n) sample to 1173 K and cooling to 323 K. (spectra **a-f** were taken in the gas mixture; spectra **g-o** were taken in vacuum)

SO_x exposure on 10Fe/20Ba/Al at 323 K (Figure 13, spectrum *a*) reveals a broad band between 1000 and 1150 cm^{-1} which indicates the presence of sulfites on different domains as it occurs also on the 5Fe/20Ba/Al sample. After the temperature of the sample is increased to 573 K in SO_x (g) (Figure 13, spectrum *c*), the features at 1041 cm^{-1}, 1230 cm^{-1} and 1353 cm^{-1} become distinguishable. These features are attributed to bulk barium sulfates, sulfates on FeO_x and overlap of sulfates on Al_2O_3 and FeOx, respectively. These features continue to grow until the temperature is increased to 773 K (Figure 13, spectrum *e*) with the appearance of a new band at 1156 cm^{-1} (bulk barium sulfate). Furthermore, the 1230 cm^{-1} feature (sulfates on FeO_x) is less pronounced at 773 K. After the sample is flashed to 873 K in SO_x (g) (Figure 13, spectrum *f*), significant changes occur in the line shape of the spectrum. The band at 1040 cm^{-1} which corresponds to bulk barium sulfates decreases in intensity. Moreover, the 1156 cm^{-1} band which also corresponds to bulk barium sulfate disappears and two additional bands are distinguished at 1117 cm^{-1} and 1180 cm^{-1}. These new features are attributed surface and bulk aluminium sulfates as discussed previously for 5Fe/20Ba/Al sample. The spectrum shape does not show a significant change until the temperature is increased to 973 K in vacuum (besides the attenuation of the 1353 cm^{-1} feature due to surface alumina sulfates). After the annealing of the sample to 973 K in vacuum (Figure 13, spectrum *m*), the features at 1290 cm^{-1} and 1240 cm^{-1} becomes visible. These bands are due to the presence of bulk barium sulfate. With the further heating of the sample to 1073 K (Figure 13, spectrum *n*), the intensity of the signal at 1040 cm^{-1} drops dramatically pointing the decomposition of barium sulfates. It is worth mentioning that even after annealing in vacuum at 1173 K, some high stable sulfate/sulfite features still exist on the surface.

Increasing Fe loading from 5wt% to 10wt% for samples containing 20wt% Ba, results in the formation of more bulk barium sulfate. Sulfates on FeO_x are less pronounced for 10 Fe/20Ba/Al due to the high intensity of the overlapping broad bands corresponding to barium and aluminium sulfates. In addition, bulk aluminium sulfates are observed to be more pronounced and their decomposition occurs at a slightly higher temperature.

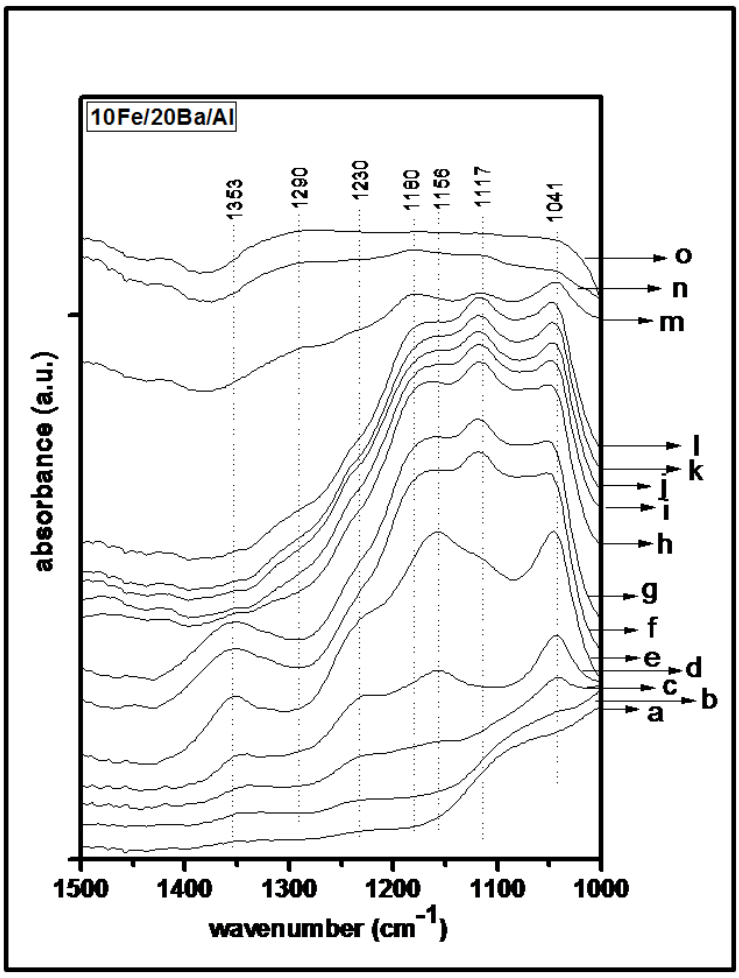

Figure 13. FTIR spectra for 0.6 Torr SO_2+O_2 (1:10) adsorption on 10Fe/20Ba/Al. **a)** After 15 min exposure to SO_2+O_2 at 323 K, **b)** after flashing the (a) sample to 473 K and cooling to 323 K, **c)** after flashing the (b) sample to 573 K and cooling to 323 K, **d)** after flashing the (c) sample to 673K and cooling to 323 K, **e)** after flashing the (d) sample to 773 K and cooling to 323 K, **f)** after flashing the (e) sample to 873 K and cooling to 323 K, **g)** after evacuation of the reactor ($P_{reactor} < 1\times10^{-4}$ Torr), **h)** after flashing the (g) sample to 473 K and cooling to 323 K, **i)** after flashing the (h) sample to 573 K and cooling to 323 K, **j)** after flashing the (i) sample to 673 K and cooling to 323 K, **k)** after flashing the (j) sample to 773 K and cooling to 323 K, **l)** after flashing the (k) sample in to 873 K and cooling to 323 K, **m)** after flashing the (l) sample to 973 K and cooling to 323 K, **n)** after flashing the (m) sample to 1073 K and cooling to 323 K, **o)** after flashing the (n) sample to 1173 K and cooling to 323 K. (spectra **a-f** were taken in the gas mixture; spectra **g-o** were taken in vacuum.)

3.2 Influence of SO_2 poisoning on the NO_2 adsorption behavior of the Fe/Ba/Al Systems via FTIR

The influence of sulfur poisoning on the NO_x adsorption behavior of the 5(10)Fe/8(20)Ba/Al samples were analyzed via IR spectroscopy. The NO_x storage performances/capacities of both fresh and poisoned samples were investigated.

All of the samples were initially saturated with 8 Torr of NO_2, FTIR spectra were acquired and then adsorbed NO_x species were removed by annealing the sample to 1023 K in vacuum. Next, samples were exposed to SO_2+O_2 (P_{Total}=0.6 Torr) gas mixture to be poisoned and the samples were saturated with 8 Torr of NO_2 for the second time and FTIR spectra were acquired. The comparison of these spectra reveals information regarding the effect of sulfur poisoning on the NO_2 adsorption for the investigated samples.

It should be noticed that NO_2 adsorption on freshly prepared Fe promoted Ba/Al storage systems were investigated using FTIR previously by Kayhan et al. [60]. It was shown that NO_2 adsorption on fresh 8Ba/Al sample results in the formation of surface and bulk nitrates. Surface bidentate nitrates were characterised with the features at 1585 cm^{-1}, 1565 cm^{-1} and 1300 cm^{-1}. The additional bands at 1320 cm^{-1} and 1440 cm^{-1}were attributed to bulk nitrates. Addition of 5wt% Fe to Ba/Al storage material reveals a different spectrum as a result of NO_2 adsorption on 5Fe/8Ba/Al sample. Intensity of the bands corresponding to the bidentate nitrates increases as a result of Fe addition. Luo et al. reported that the introduction of Fe into the Ba/Al system leads to a decrease in the formation of bulk BaO which hinders the formation of $BaAl_2O_4$ sites [56]. Hence, it was proposed that the presence of 5 wt% Fe loading enhances the bidentate nitrates by lowering the formation of $BaAl_2O_4$ phase in 5Fe/8Ba/Al sample [60]. It was reported also that Fe promotion creates additional NO_x storage sites and that NO_x is stored as bidentate nitrates on FeO_x domains [60]. Increasing Fe loading to 10wt% in Ba/Al system leads to a decrease in the intensity of bands related to bidentate surface nitrates, which might be due to the fact that surface area of Ba/Al system reduces via sintering as the amount of Fe

increased to 10wt%. Moreover, the crystallite size of Fe domains increases as Fe content of the Ba/Al system increases.

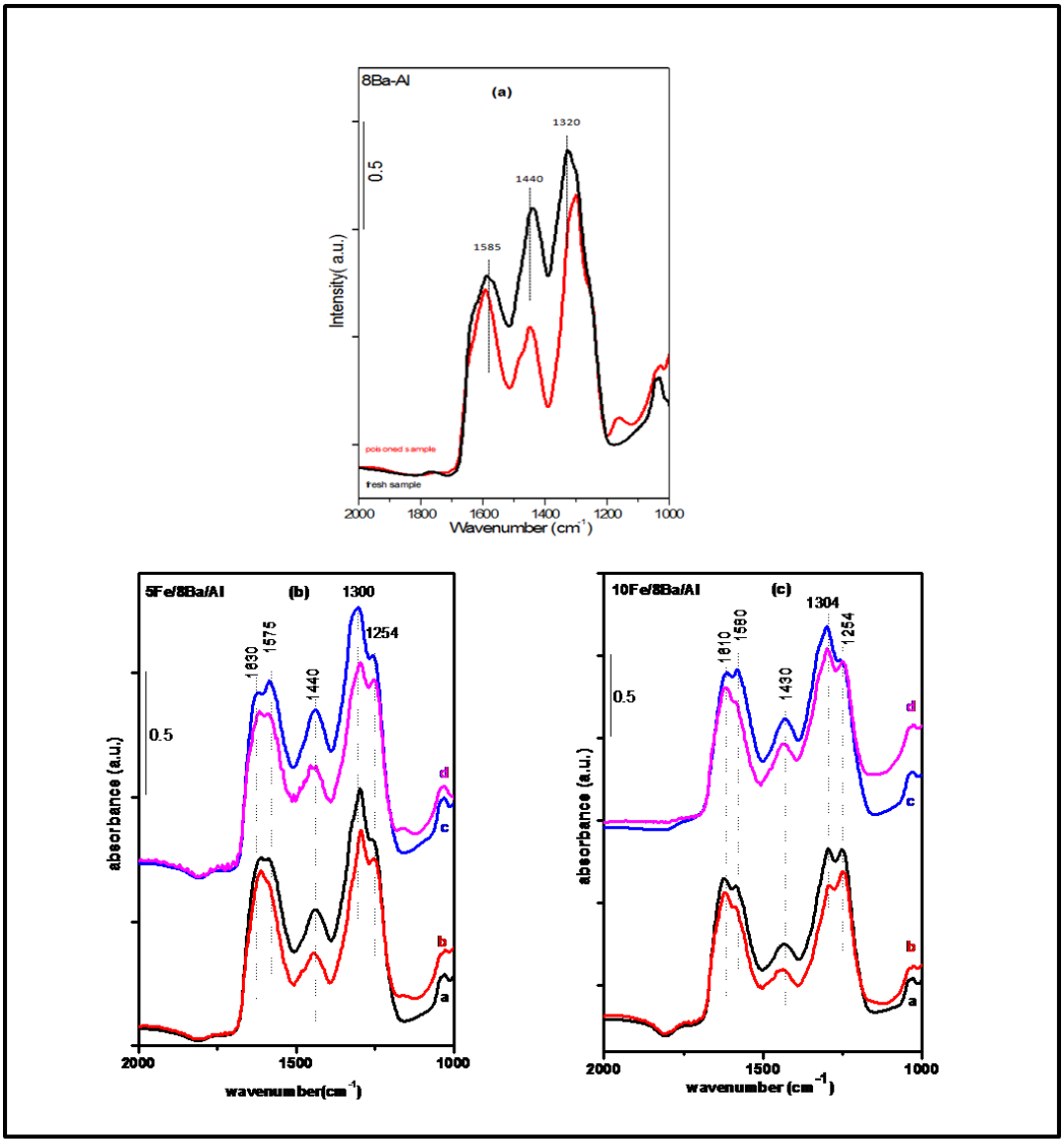

Figure 14. FTIR spectra corresponding to 8 Torr of NO_2 adsorption at 323 K on fresh (black and blue spectra) and poisoned (red and purple spectra) **a)** 8Ba/Al, **b)** 5Fe/8Ba/Al, **c)** 10Fe/8Ba/Al 323 K. (red spectra correspond to poisoning of the sample at 473 K; purple spectra correspond to poisoning at 673 K.)

Figure 14 shows the FTIR spectra monitored after NO_x uptake of 8Ba/Al and 5(10)Fe/8Ba/Al samples before and after sulfation. It is clear that for the 8Ba/Al sample, the intensity of the bands corresponding to both surface and bulk nitrates decreases after sulfation *(red spectrum).* This decline is more pronounced for bulk nitrates (1460 cm^{-1}), whereas it is less visible for surface nitrates on BaO and nitrates on alumina (1585 cm^{-1}, 1565 cm^{-1} and 1300 cm^{-1}). Apparently, SO_x species bound to the surface inhibit the nitrate diffusion through the inner part of BaO domains, hence formation of bulk nitrates is suppressed.

Figure 14 (b) shows the NO_x uptake capacity of 5Fe/8Ba/Al sample before *(spectra a and c)* and after *(spectra b and d)* SO_x poisoning. Compared to 8Ba/Al sample, 5Fe/8Ba/Al sample shows a smaller decrease in band intensities of both surface and bulk nitrates. Bulk nitrates (1441 cm^{-1}) are obviously less affected by sulfur poisoning in case of 5Fe/8Ba/Al sample. Since the bands related to the nitrates on FeO_x and BaO domains overlap between 1585-1614 cm^{-1}, it can be stated that nitrates on both surface BaO and FeO_x domains are partially suppressed. The poisoning of the samples was performed at two different temperatures (473 K and 673 K) in order to investigate the influence of temperature on sulfur poisoning. The comparison of the spectra recorded after NO_2 uptake of the poisoned samples at different temperatures *(473 K, spectra b; 673 K, spectra d)* shows that sulfur poisoning is more effective at the higher temperature (673 K).

Poisoning of 10Fe/8Ba/Al sample is shown in Figure 14 (c). Increasing Fe content to 10wt% leads to increased sulfur uptake. Comparison of the relative ratio of the areas under the spectrum *b* and *a* in Figure 14 (b) (5Fe/8Ba/Al) to the ratio of the areas under the spectrum *b* and *a* in Figure 14 (c) (10Fe/8Ba/Al) clearly shows that both surface and bulk nitrates are affected to a greater extent from sulfur poisoning in 10Fe/8Ba/Al. Compared to surface nitrates, bulk nitrates are also observed to be more affected from sulfur poisoning as Fe content is increased from 5wt% to 10wt%. It is also worth mentioning that poisoning effect is more pronounced for 10Fe/8Ba/Al sample at higher temperature (Figure 14 (c), *spectra c and d*).

Figure 15 (a) shows the NO_x uptake capacity of 20Ba/Al sample before *(black spectrum)* and after *(red spectrum)* sulfation. The features at 1610 cm^{-1} and 1265 cm^{-1}, which correspond to nitrates on alumina, are less visible for 20Ba/Al

sample. This is associated with the covering of the alumina sites by the BaO domains with increasing loading of BaO [61-65].

As in the case of 8Ba/Al sample, NO_x uptake capacity of 20Ba/Al sample is affected from sulfur poisoning which is evident by the decline in the intensities of the bands corresponding to both surface and bulk nitrates (Figure 15 (a), *red spectrum*). In case of 8Ba/Al sample, suppression of surface nitrates is not pronounced as much as that of bulk nitrates; on the other hand, band intensities of both surface and bulk nitrates are reduced drastically for 20Ba/Al sample.

Figure 15 (b) shows the NO_2 adsorption on 5wt% Fe loaded 20Ba/Al sample. As in the case of 5Fe8Ba/Al sample, presence of Fe loading enhances the bands associated with bidentate nitrates. Increasing of Fe content to 10wt% in 20Ba/Al sample (Figure 15 (c)) results in a minor decrease in the intensity of bidentate surface nitrates compared to the 5Fe/20Ba/Al sample. This could be explained by the sintering of the Fe sites with increasing Fe loading. Moreover, higher Fe loading may change the interaction between the Ba sites and the alumina surface leading to more bulk BaO morphology and increased $BaAl_2O_4$ formation [60].

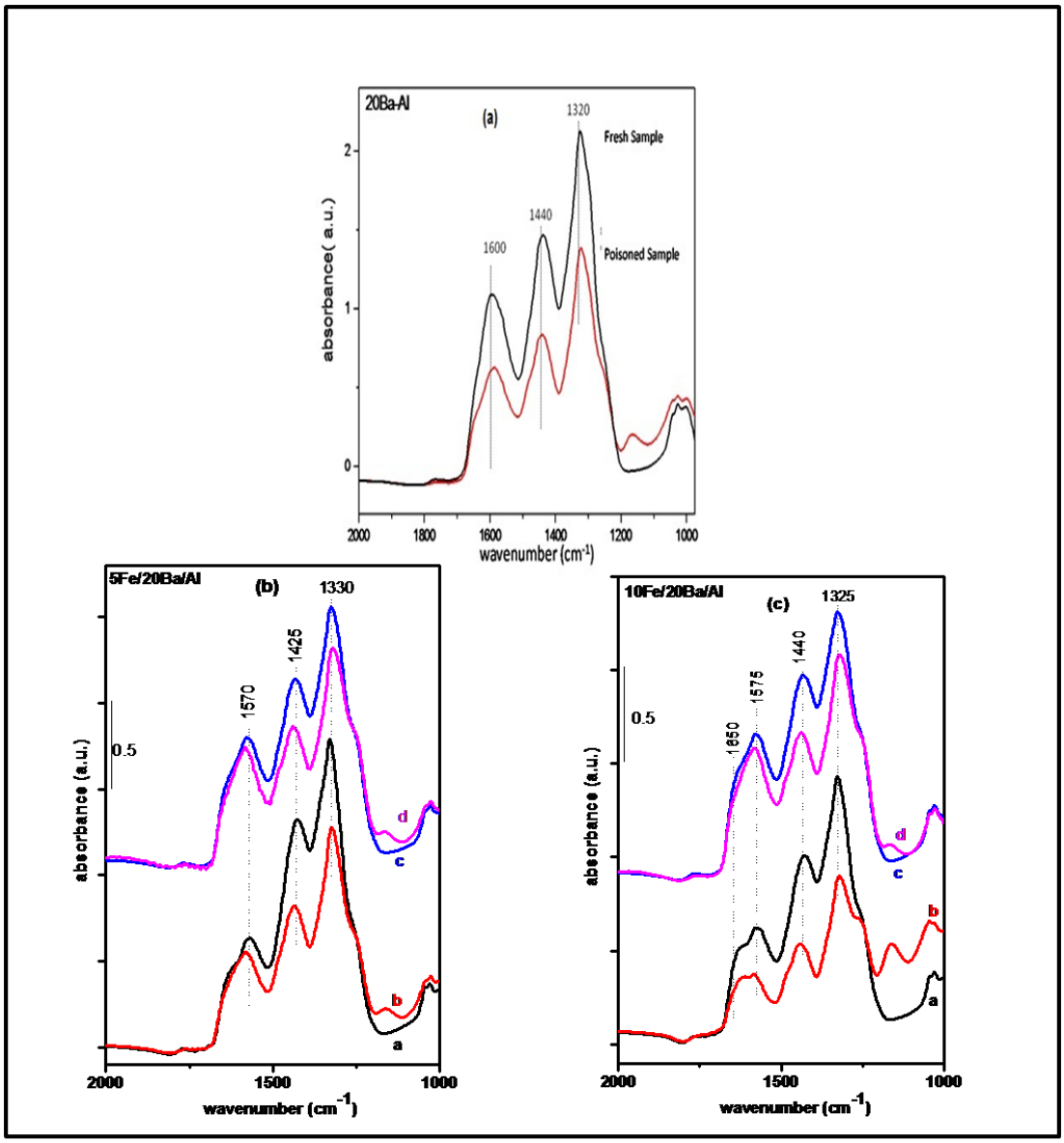

Figure 15. FTIR spectra corresponding to 8 Torr of NO_2 adsorption at 323 K on fresh (black and blue spectrum) and poisoned (red and purple) **a)** 20Ba/Al, **b)** 5Fe/20Ba/Al, **c)** 10Fe/20Ba/Al 323 K. (red spectra correspond to poisoning of the sample at 473 K; purple spectra correspond to poisoning at 673 K.)

Compared to the 20Ba/Al system, Figure 15 indicates that 5Fe/20Ba/Al system is affected from sulfur poisoning by a marginally smaller extent while the response to 10Fe/20Ba/Al is very similar to 20/Ba/Al. Analysis of Figures 14 and 15 reveals that for low Ba loadings (i.e. 8 wt%), Fe addition has a positive influence on the NO_x uptake in the presence of sulfur while for high Ba loadings (i.e. 20 wt%), Fe promotion has almost no positive influence on NO_x storage in the presence of sulfur. These results are also consistent with the NO_x TPD experiments performed on fresh and poisoned 5(10)Fe/8(20)Ba/Al samples given in Figures 17 and 18 below.

3.3 Thermal stability of the adsorbed NO_x species on the SO_x treated Fe/Ba/Al support materials

In order to investigate the influence of SO_x adsorption on the thermal behaviour and the desorption properties of the NO_x species on Fe/Ba/Al system, TPD experiments were performed.

Figure 16 shows the NO_x desorption profiles from the poisoned and fresh γ-Al_2O_3 surface which is saturated with NO_2 as described in the experimental section. For clarity, only the 30, 32 and 46 amu desorption channels are shown. For the fresh alumina surface, two major desorption features are observed. In the light of the studies in literature [61,63,66,67] the first NO_x desorption feature visible at 404 K is related to desorption of weakly bound NO^+ and/or N_2O_3, which desorb in the form of NO_2 and $NO+O_2$. The main desorption feature appearing at 742 K corresponds to desorption/decomposition of bridging and bidentate nitrates yielding a significant NO_2 desorption signal.

The SO_x adsorption on the alumina surface has a significant influence on the NO_x desorption features (Figure 16 (b)). The desorption peak appeared at 1107 K, which was not observed in previous experiment, is related to desorption of NO_x from sample holder. This high temperature desorption feature is observed for all samples when the temperature ramp is extended up to 1200 K during the TPD runs. In Figure 16, it is apparent that, the high temperature desorption feature at c.a. 730-740 K is suppressed after sulfur poisoning indicating that sulfates are competing with nitrates

for surface sites, however weakly bound N_2O_3 or NO^+ speices are not significantly affected by sulfation. It should be noted that oxidation of SO_2 to sulfates can be achieved not only by O_2, but also by NO_2. One of the possible pathways for the interaction of SO_x species with adsorbed NO_x species is the following:

$$SO_3^{2-}\,(ads) + NO_2\,(ads, g) \rightarrow SO_4^{2-}\,(ads) + NO\,(g) \qquad (1)$$

$$SO_3^{2-}\,(ads) + 2\,NO_2\,(ads, g) \rightarrow SO_4^{2-}\,(ads) + N_2O_3\,(ads) \qquad (2)$$

$$N_2O_3\,(ads) \rightarrow NO_2^-\,(ads) + NO^+\,(ads) \qquad (3)$$

This pathway explains the formation of sulfate species in the result of oxidation of sulfites by NO_2, and the formation of weakly adsorbed NO^+ and/or N_2O_3.

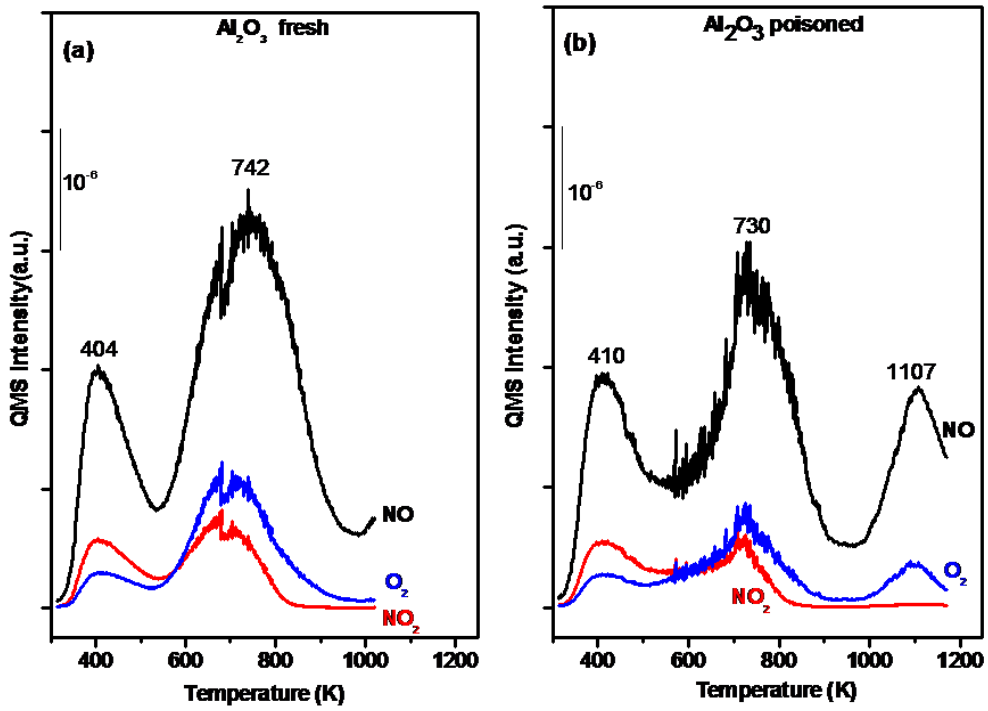

Figure 16. TPD profiles obtained from fresh **(a)** and poisoned **(b)** ɤ-Al_2O_3 samples which are saturated with 8 Torr NO_2 (g) at 323 K for 15 minutes. Black, blue and red curves correspond to 30 amu (NO), 32 amu (O_2) and 46 amu (NO_2) signals, respectively. (Sample was saturated first with 8 Torr of NO_2 at 323 K, followed by evacuation of the reactor. After that, the sample was flashed to 1023 K during TPD experiment. Then, the sample was poisoned by SO_2 +O_2 (P_{Total}= 0.6 Torr) gas mixture at 323 K, followed by further heating in the gaseous mixture at 673 K for 30 minutes. After evacuation of gaseous mixture, sample was flashed to 1173 K during second TPD)

Another pathway in which surface nitrate species facilitate the oxidation of surface sulfites or weakly adsorbed molecular SO_2 species is the following:

$$3NO_2\,(g) + O^{2-}\,(s) \rightarrow 2\,NO_3^-\,(ads) + NO\,(g) \quad (4)$$

$$SO_3^{2-}\,(ads) + NO_3^-\,(ads) \rightarrow SO_4^{2-}\,(ads) + NO_2^-\,(ads) \quad (5)$$

$$NO_2^-\,(ads) + NO_2\,(ads, g) \rightarrow NO_3^-\,(ads) + NO\,(g) \quad (6)$$

$$NO_2^-\,(ads) + 2\,NO_2\,(ads, g) \rightarrow NO_3^-\,(ads) + N_2O_3\,(ads) \quad (7)$$

Figure 17 (a and b) shows TPD profiles of 8Ba/Al sample upon NO_2 adsorption before and after sulfur poisoning. As mentioned previously, the signal at 390 K is related to decomposition of the N_2O_3/NO^+ species [60,65,66]. This signal is less intense compared to the one observed for Al_2O_3 support material, which may be due to the fact that BaO domains cover some of the surface of support in 8Ba/Al sample and these species are formed predominantly on alumina. The main desorption feature appearing at 700 K is due to the decomposition of the surface bidentate nitrates on BaO domains. The other desorption feature which is seen as a shoulder at 820 K is attributed to bulk nitrates. Higher desorption temperature of bulk nitrates points that bulk nitrates are more stable than surface nitrates. It should be noted that decomposition of the bulk nitrates occur via NO + O_2 desorption, whereas decomposition of surface nitrates yields mostly NO_2. The comparison of the total NO_x storage indicates that NO_x adsorption capacity is significantly enhanced for 8Ba/Al with respect to the pure Al_2O_3 support material.

SO_x adsorption on 8Ba/Al surface (Figure 17 (b)) increases the desorption of weakly adsorbed N_2O_3/NO^+ species, while the intensity of the signals corresponding to desorption of both bulk and surface nitrates (700 K and 820 K) decrease simultaneously. Since the TPD line shape and the nature of the decomposition products are rather unchanged (besides a total attenuation of all desorption intensities) upon sulfur poisoning, it can be argued that sulfur poisoning is non-preferential on 8Ba/Al surface influencing both BaO and Al_2O_3 domains.

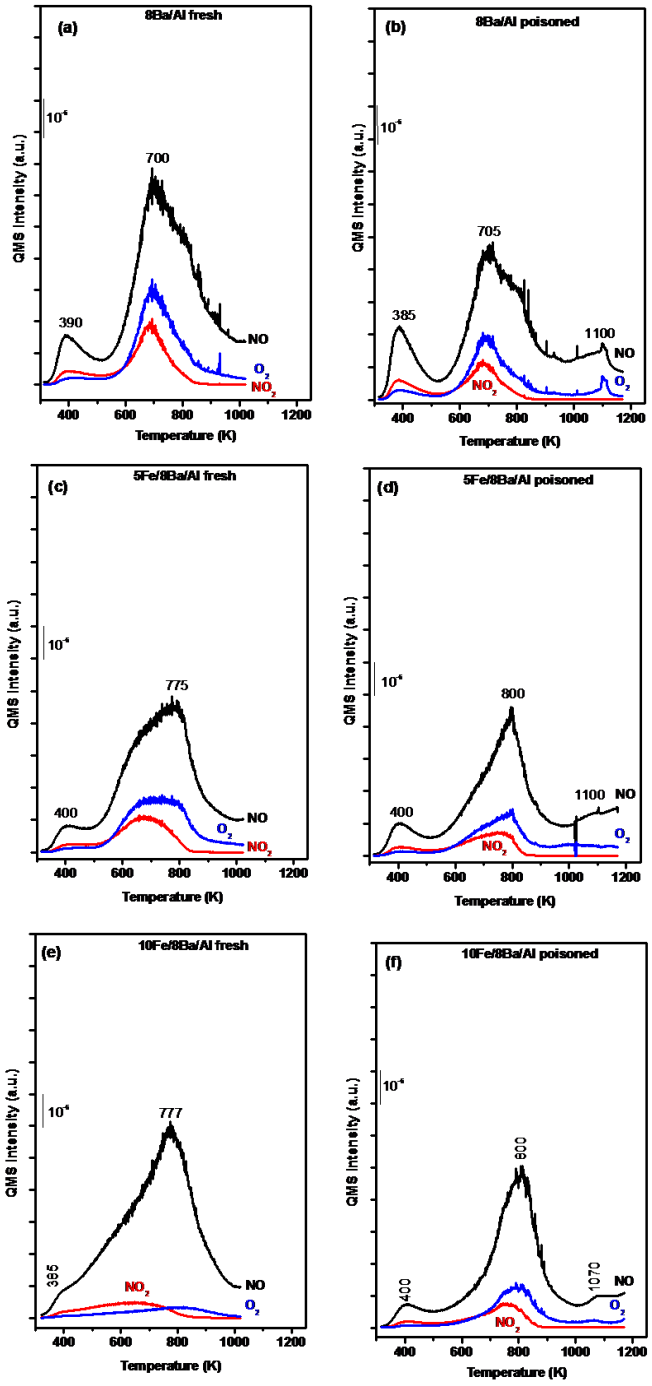

Figure 17. TPD profiles obtained from fresh **(a)** and poisoned **(b)** 8Ba/Al; fresh **(c)** and poisoned **(d)** 5Fe/8Ba/Al; and fresh **(e)** and poisoned **(f)** 10Fe/8Ba/Al samples which are saturated with 8 Torr NO_2 (g) at 323 K for 15 minutes. Black, blue and red curves correspond to 30 amu (NO), 32 amu (O_2) and 46 amu (NO_2) signals, respectively.

In Figures 17c and 17d, the NO_2 desorption profiles are shown for the 5Fe/8Ba/Al sample before and after SO_x poisoning. The main difference in desorption profile of the 5Fe/8Ba/Al sample compared to the one observed for 8Ba/Al sample is an increase in the desorption signal at relatively high temperatures yielding an asymmetrical feature appearing at 775 K. This high temperature feature is most probably due to the decomposition of nitrate species on FeO_x sites as well as bulk BaO domains. Besides the major signal at 775 K, the signals at 400 K, 630 K and 685 K also exist. These features are attributed to desorption of N_2O_3/NO^+, nitrates on Al_2O_3 and bidentate surface nitrates on surface BaO domains, respectively.

After SO_x poisoning of the 5Fe/8Ba/Al sample (Figure 17d), intensity of the feature at 400 K (weakly bound N_2O_3/NO^+) increases marginally, while the broad desorption signal associated with the nitrates on FeO, Al_2O_3 and BaO assumes an asymmetrical line shape presenting a preferential attenuation of its desorption signal within 600-700 K. This observation suggests that sulfur poisoning has a less pronounced influence on the highly stable bulk nitrates on BaO sites for the 5Fe/8Ba/Al sample in line with the IR results given in Figure 14.

Figure 17e and 17f shows TPD profiles of the 10Fe/8Ba/Al sample upon NO_2 adsorption. The general observations are in line with the 5Fe/8Ba/Al sample. It can be noted that for the fresh 10Fe/8Ba/Al sample, additional NO_x desorption features also exist within 400-600 K due to higher Fe loading. These desorption features could be associated with weakly bound molecular NO_2 or nitrates on FeO_x domains which are heavily suppressed after SO_x poisoning. It is worth mentioning that as in the case of 5Fe/8Ba/Al, high temperature desorption features (775-800 K) in the TPD data of 10Fe/8Ba/Al also seem to be resilient against sulfur poisoning.

Figure 18 (a and b) shows NO_x desorption profiles of 20Ba/Al before and after sulfur poisoning, respectively. The major desorption feature at 790 K lies at a higher temperature compared to the major desorption feature for the 8Ba/Al sample located at 700 K. This difference in the decomposition temperature is associated with the presence of bigger BaO agglomerates on the 20Ba/Al sample which can form more bulk-like nitrates. TPD profile of 20Ba/Al sample upon NO_2 adsorption after SO_x poisoning is shown in Figure 18b. The low temperature feature at 385 K (N_2O_3, NO^+) increases in intensity as in the case of the 8Ba/Al sample. Comparison of the

TPD signals for fresh vs. poisoned samples of 8Ba/Al and 20 Ba/Al shows that 20Ba/Al is affected more significantly by the SO_2 poisoning in terms of NO_x uptake capacity.

An overall analysis of the TPD spectra given in Figure 18a-16f reveals that sulfur poisoning does not significantly alter the relative abundances of different types of NO_x species on the surface and suppresses all of the stored NO_x species in a rather non-preferential manner. This is evident from the preservation of the line shapes as well as the decomposition product distributions seen in the $NO/NO_2/O_2$ channels in Figures 18a-f. It is also visible in Figures 16a, 16c and 16e that addition of 5 wt% Fe may have a minor positive effect on the total NO_x uptake while the addition of 10 wt% Fe has a slightly negative effect on the total NO_x storage, probably due to enhanced sintering leading to the loss of exposed surface sites in the latter case.

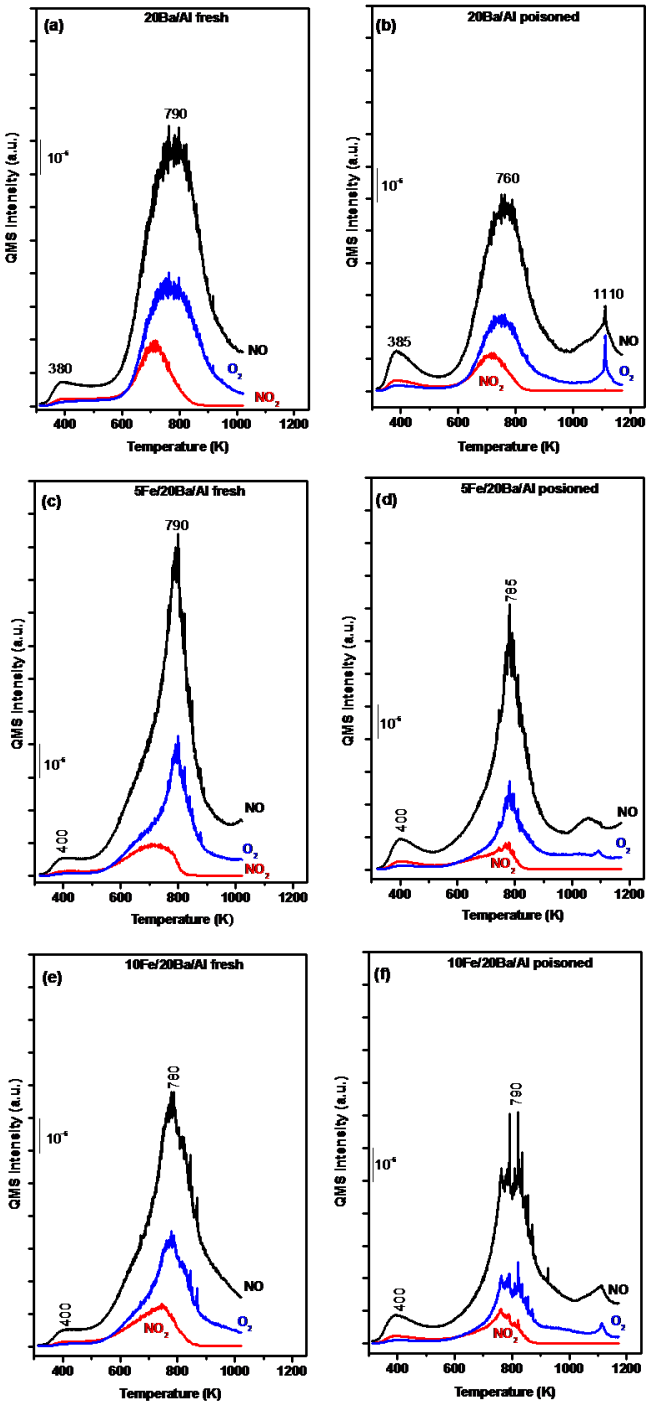

Figure 18. TPD profiles obtained from fresh **(a)** and poisoned **(b)** 20Ba/Al; fresh **(c)** and poisoned **(d)** 5Fe/20Ba/Al; and fresh **(e)** and poisoned **(f)** 10Fe/20Ba/Al samples which are saturated with 8 Torr NO_2 (g) at 323 K for 15 minutes. Black, blue and red curves correspond to 30 amu (NO), 32 amu (O_2) and 46 amu (NO_2) signals, respectively.

3.4 Thermal stabilities of the adsorbed SO_x species on the Fe/Ba/Al materials

After analyzing the thermal stability of the stored NO_x species on the surface of Fe/Ba/Al samples before and after sulfur poisoning, in this chapter the thermal behaviour of SO_x on the Fe/Ba/Al surfaces will be investigated. The TPD spectra presented here correspond to the same experiments considered in the previous chapter. SO_2 (m/z = 64), SO (m/z= 48) and H_2S (m/z = 34) signals were monitored for each sample spectrum. Alumina support material, 8Ba/Al and 20 Ba/Al are also investigated as benchmark samples.

Figure 19 shows the desorption profiles of SO_2, SO and H_2S from γ-Al_2O_3 sample. There are two desorption signals. The low temperature feature at 655 K is due to the desorption weakly bound molecular SO_2 species and/or sulfites. The dominant desorption signal is located at c.a. 1000 K and is attributed to the strongly bound surface and bulk sulfates on alumina. H_2S desorption is negligible for all samples in Figures 19-21.

Desorption profiles of SO_x species from 8Ba/Al, 5Fe/8Ba/Al and 10Fe/8Ba/Al are shown in Figure 20. The low temperature SO and SO_2 desorption features appear at 540 K for the 8Ba/Al sample (Figure 20, *a*), while the high temperature desorption feature is located at 1100 K as in the case of SO_x desorption from pure alumina surface. On the other hand, it should be noted that the high temperature desorption feature in Figure 20 *a* has a low-temperature tail which may be associated with sulfates on “surface” BaO sites. This observation suggests that the stability of the sulfates formed on the “bulk” BaO sites have a similar thermal stability to that of the sulfates formed on the alumina support material while the sulfates formed on surface BaO domains are thermally less stable by a small margin. 5Fe/8Ba/Al sample reveals a desorption profile (Figure 20, *b*) consisting of two main features as in the cases of alumina and 8Ba/Al. The minor feature corresponding to the weakly bound sulfites and molecular SO_2 is evident at 525 K. The major desorption signal for 5Fe/8Ba/Al appears as a complex broad peak within 900-1200 K. It is worth mentioning that in the absence of BaO, the major SO_x desorption takes place at c.a. 1017 K for the 5Fe/Al sample (data not shown). This observation

indicates that the broadening of the SO_x desorption feature (particularly towards low desorption temperatures) for the 5Fe/8Ba/Al sample given in Figure 20 *b* is due to the presence of sulfates on FeO_x sites and/or the sulfates on "surface" BaO domains which are formed due to the morphological changes occurring after Fe addition. Increasing in the Fe content of the 8Ba/Al system to 10wt% reveals a desorption profile (Figure 20, *c*) consisting of features at 525 K (weakly bound sulfite and molecular SO_2), a shoulder at 900 K (sulfates on FeO_x domains and on surface BaO domains), a peak at 1070 K (sulfates on bulk BaO domains and on alumina support sites) and an incomplete desorption feature with a desorption maximum located at T > 1200 K (possibly due to highly stable sulfates on BaO sites generated after Fe promotion). Thus it can be argued that Fe addition leads to low-temperature SO_x desorption signals within 800-1070 K which may be attributed to sulfates on FeO_x domains and/or surface BaO domains. In addition, Fe addition also results in a SO_x desorption feature having a desorption maximum much higher than Ba/Al samples.

Desorption profiles of SO_x species from 20Ba/Al, 5Fe/20Ba/Al and 10Fe/20Ba/Al are shown in Figure 21. Desorption of SO_x species from 20Ba/Al (Figure 21, *a*) presents a major desorption maximum at 1100 K which is very similar to that of 8Ba/Al however with a significantly larger main SO_x desorption signal. . This peak is attributed to sulfates desorbing from both sulfates originating from bulk BaO and Al_2O_3 sites while the low-temperature tail of this feature can be associated with sulfates on surface BaO sites. As expected, increasing the Ba loading from 8wt% (Figure 20 *a*) to 20wt% (Figure 21 *a*) in the Ba/Al system increases the total sulfur uptake due to the increasing surface concentration of basic alkaline-earth oxide domains with a high affinity towards SO_x.

Addition of 5wt% Fe to 20Ba/Al system shows a significant difference in SO_x desorption profile (Figure 21, *b*). In addition to the weak signal at 525 K and intense peak at 1093 K (as discussed above), a well-defined desorption peaks becomes visible which can be attributed to sulfate desorption from FeO_x domains. It can be noticed that SO_x desorption from FeO_x domains becomes more discernable for 20Ba/Al systems. In addition to these features an incomplete desorption feature might also exist at T > 1200 K which can be associated with highly stable sulfates formed after Fe addition.

Increasing Fe content to 10wt% for 20Ba/Al system results in a desorption profile (Figure 21 *c*) which is very similar to that of 5Fe/20Ba/Al. For 20Ba/Al system, the increasing of Fe content from 5wt% to 10 wt% does not lead to a significant difference in the desorption profiles of SO_x species, whereas this effect leads to noticeable changes for the 5(10)Fe/8Ba/Al systems.

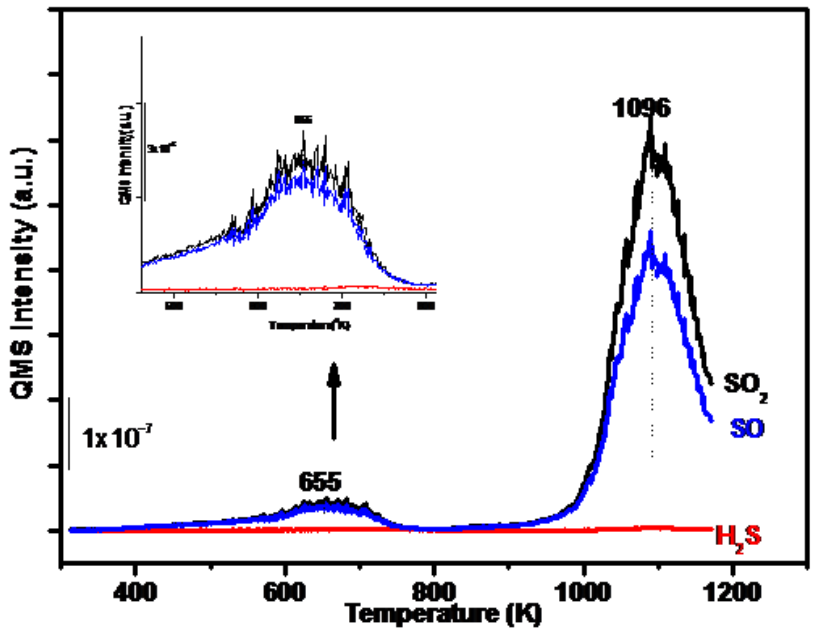

Figure 19. Desorption profile of SO_2, SO and H_2S for γ-Al_2O_3. (The sample was poisoned by 0.6 Torr of SO_2+O_2 gas mixture at 323 K, followed by heating of the sample in gaseous mixture at 673 K for 30 minutes. After evacuation, sample was flashed to 1173 K during TPD experiment)

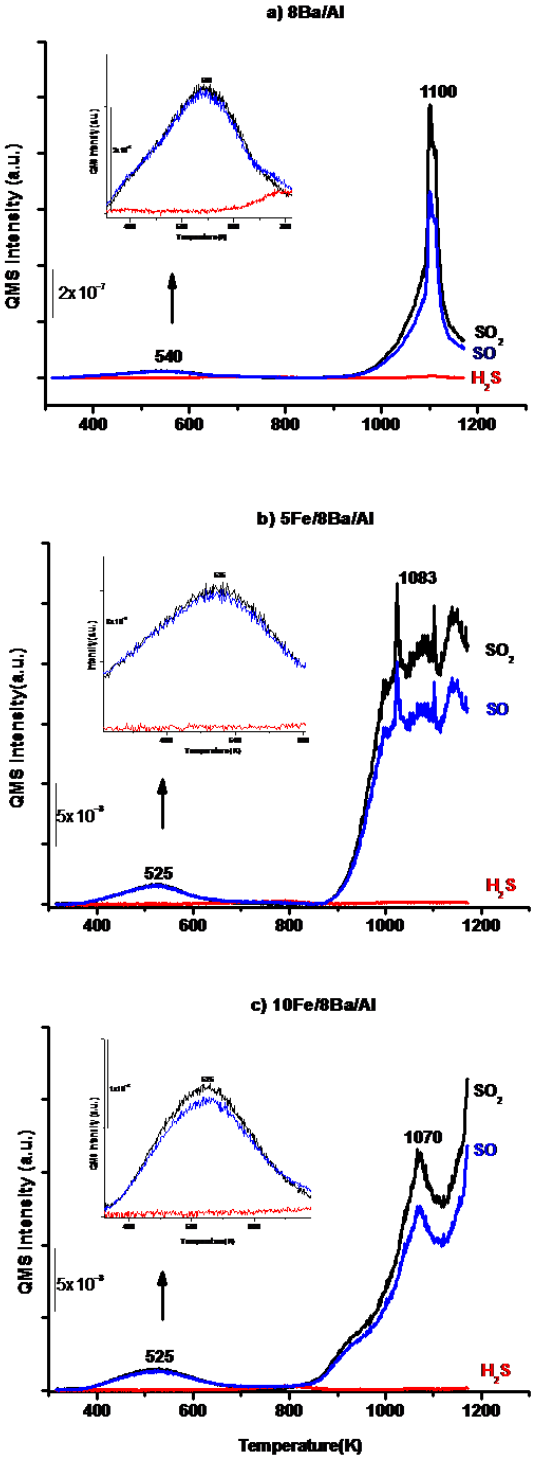

Figure 20. Desorption profile of SO_2, SO and H_2S for **a)** 8Ba/Al, **b)** 5Fe/8Ba/Al, and **c)** 10Fe/8Ba/Al. (The sample was poisoned by 0.6 Torr of SO_2+O_2 gas mixture at 323 K, followed by heating of the sample in gaseous mixture at 673 K for 30 minutes. After evacuation, sample was flashed to 1173 K during TPD experiment.)

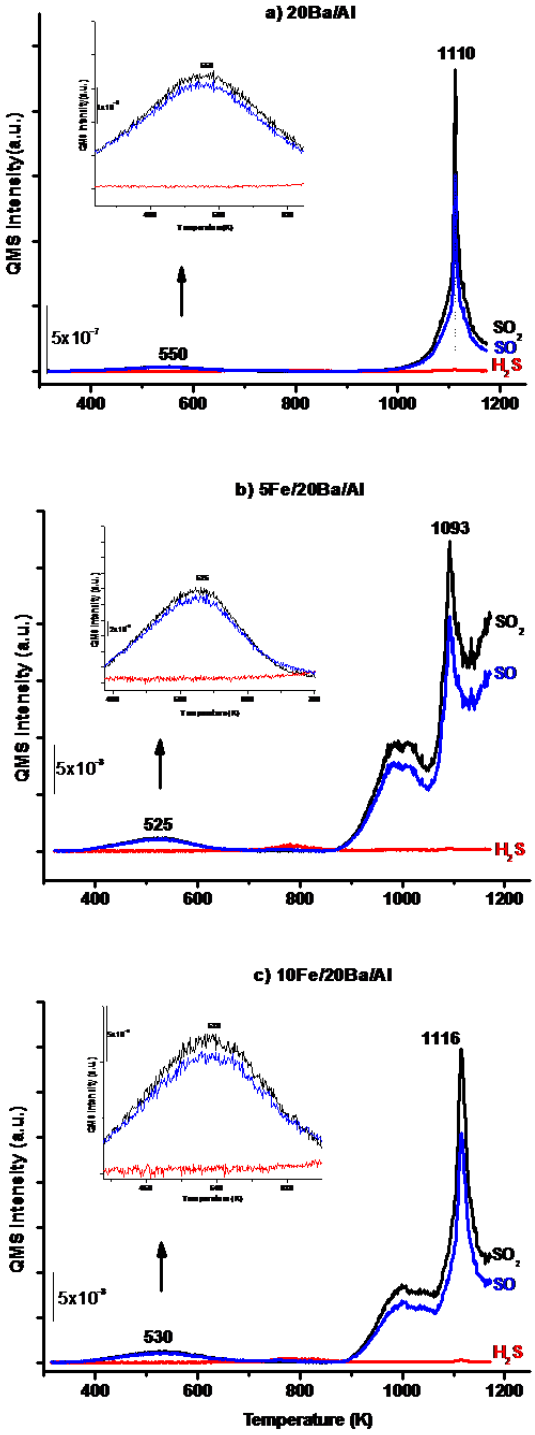

Figure 21. Desorption profile of SO_2, SO and H_2S for **a)** 20Ba/Al, **b)** 5Fe/20Ba/Al, and **c)** 10Fe/20Ba/Al. (The sample was poisoned by 0.6 Torr of SO_2+O_2 gas mixture at 323 K, followed by heating of the sample in gaseous mixture at 673 K for 30 minutes. After evacuation, sample was flashed to 1173 K during TPD experiment.)

3.5 XPS analysis of the poisoned Fe/Ba/Al storage materials

In order to quantitatively compare the amount of SO_x stored on the investigated surfaces, XPS analysis of the poisoned samples was performed. Because of the relatively low sensitivity of the XPS technique towards sulfur, poisoning procedure was modified to obtain better S/N and more accurate atomic ratio values. Thus, before the atomic ratio determination by XPS, the samples were poisoned in 10 Torr of SO_x (SO_2:O_2 = 1: 10) at 673 K for 30 minutes.

For all samples, XPS spectrum revealed a S2p binding energy within 168-170 eV which indicates the presence of sulfates.

Figure 22 shows the atomic sulfur content on the investigated sample surfaces relative to all of the other atoms (e.g. Al, O, Ba) present. Al_2O_3 sample is observed to accumulate the least amount of sulfur, and 5Fe/20Ba/Al is demonstrated to have the highest amount of sulfur. 5wt% Fe addition to Ba/Al storage materials results in higher storage of sulfur, whereas further Fe loading (10wt%) leads to a decrease in sulfur uptake of Ba/Al systems. Table 3 demonstrates that the same trend is valid also for S/Ba atomic ratio values. It is worth mentioning that the results corresponding to the poisoning of the samples in 0.6 Torr SO_x (data not shown) demonstrate the same trend for sulfur percentage as in the case of 10 Torr of SO_x poisoning.

In the light of the studies in literature [54, 68, 69] it may be proposed that addition of Fe domains to Ba/Al systems provides favorable basic sites for adsorption of acidic SO_2, which is followed by sulfate formation.

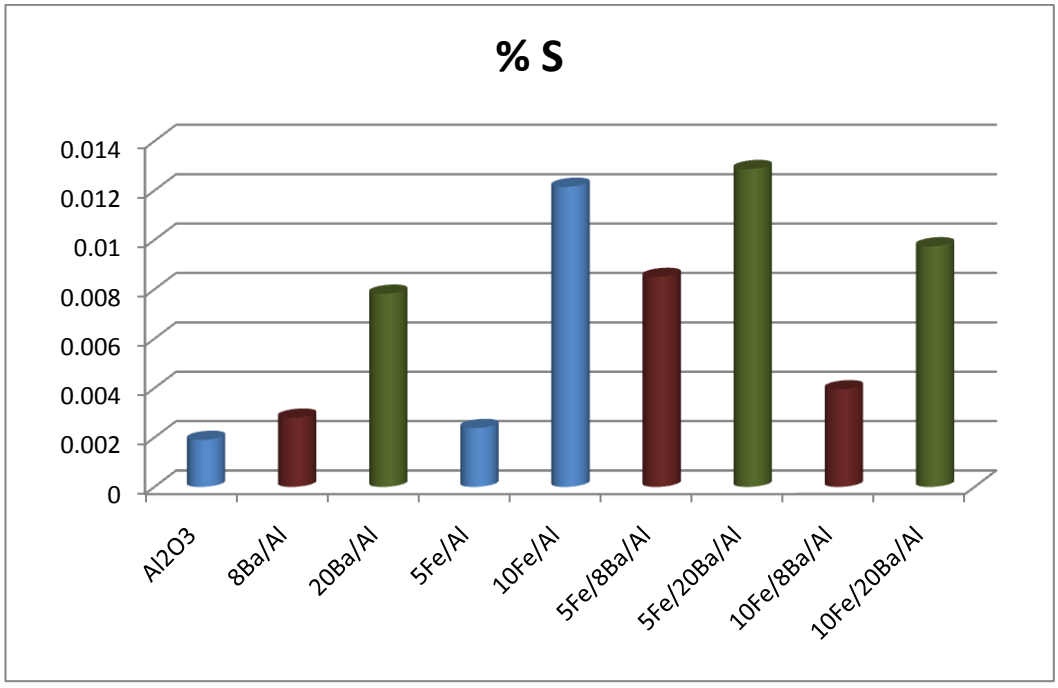

Figure 22. Schematic representation of sulfur percentage in poisoned materials obtained from XPS results.

Table 3. Surface atomic ratios for the poisoned materials obtained from XPS results

samples	**% S**	**S/Ba**
Al_2O_3	0.0019	-
5Fe/Al	0.0024	-
10Fe/Al	0.0122	-
8Ba/Al	0.0028	0.2
20Ba/Al	0.0078	0.3
5Fe/8Ba/Al	0.0085	0.7
10Fe/8Ba/Al	0.0039	0.4
5Fe/20Ba/Al	0.0129	0.5
10Fe/20Ba/Al	0.0097	0.4

3.6 SEM-EDX Measurements of the Poisoned Fe/8Ba/Al materials

SEM and EDX-elemental mapping techniques were also used to investigate the morphological changes and the elemental distribution qualitatively. Figure 21 shows the SEM-EDX images corresponding to the combination of elemental distributions of barium, iron and sulfur of the selected 5Fe/8Ba/Al and 10Fe/8Ba/Al samples.

Figure 23 (*a and b*) demonstrates the surface dispersion of sulfur, iron and barium on the 5Fe/8Ba/Al sample. Similarly, Figure 23 (*c and d*) presents the surface dispersion of same elements on the 10Fe/8Ba/Al sample. EDX elemental maps in Figure 23 (*a and c*) reveal scattered red and green islands which represent Fe and S containing domains, respectively. Similarly, Figure 23 (*b and d*) exhibits red and green islands which correspond to Ba and S containing domains, respectively. Comparison of the EDX map in Figure 23 (*a and b*) indicates that Fe domains have a better surface dispersion than Ba domains and sulfur has no noticeable particular preference on either Ba or Fe sites. Increasing the Fe content (10Fe/8Ba/Al sample given in Figures 23 (*c-d*)) reveals more yellow colored spots indicating overlapping S+Fe or S+Ba signals due to the larger SO_x uptake with higher Fe content. Apparently the low spatial resolution of the SEM-EDX technique is not capable of resolving the sulfur preference on BaO and FeO_x nano domains. A TEM-EDX study with a high spatial resolution would be beneficial to obtain the sulfur distribution map at the nanoscale.

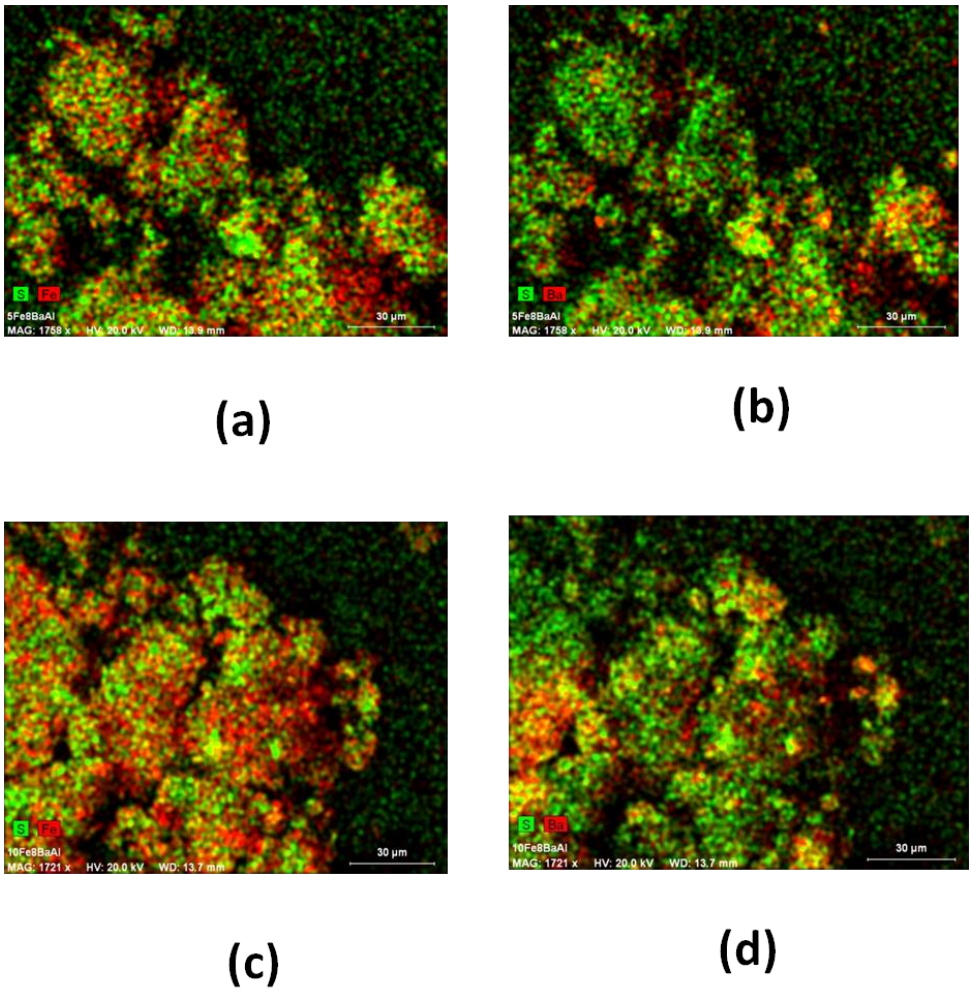

Figure 23. Fe, Ba and S elemental EDX mapping images of SO_x poisoned 5Fe/8Ba/Al and 10Fe/8Ba/Al materials. **(a)** and **(b)** represent the combined Fe-S and Ba-S elemental mappings of 5Fe/8Ba/Al, respectively; **(c)** and **(d)** show the combined Fe-S and Ba-S elemental mapings of 10Fe/8Ba/Al, respectively.

4 CONCLUSIONS

In the current work, ternary mixed oxide systems in the form of $BaO/FeO_x/Al_2O_3$ were studied with varying compositions as an alternative to the conventional NO_x storage materials (i.e. BaO/Al_2O_3). NO_x uptake properties of the freshly prepared samples, sulfur adsorption and NO_x storage in the presence of sulfur was investigated in order to elucidate the sulfur tolerance of these advanced NO_x storage systems in comparison to their conventional counterparts. In order to achieve a detailed analysis of these complex ternary systems, benchmark samples such as Al_2O_3, BaO/Al_2O_3, FeO_x/Al_2O_3 were also investigated in a similar manner.

Our main conclusions can be summarized as follows:

- Addition of FeO_x domains to the conventional BaO/Al_2O_3 system introduces additional NO_x storage sites and tends to increase the total NO_x uptake capacity.

- SO_2+O_2 adsorption on the investigated samples initially lead to the formation of sulfites at low temperatures which are converted into surface and bulk sulfates with increasing temperatures. After annealing at 1173 K in vacuum most of the sulfates can be removed from the surface and the samples can be regenerated. However, for Fe/Ba/Al samples formation of various highly-stable sulfite and sulfate species were also observed which survive on the surface even after annealing at elevated temperatures (1173 K).

- Sulfur poisoning on 5(10)Fe/8Ba/Al samples lead to preferential poisoning of the FeO_x, Al_2O_3 and surface BaO sites where bulk BaO sites seems to be more tolerant towards sulfur poisoning. In contrast, sulfur poisoning occurs in a rather non-preferential manner on the 5(10)Fe/20Ba/Al samples influencing all of the NO_x storage sites.

- Thermal stability of the sulfate species seem to increase in the following order: surface alumina sulfates < surface Ba sulfates ≈ Fe sulfates < bulk Ba sulfates ≈ bulk alumina sulfates < highly stable sulfates and sulfites on Fe/Ba/Al surfaces.

- In overall, it can be argued that the Fe promotion has a positive influence on the NO_x storage capacity as well as a positive effect on the sulfur tolerance when the Ba loading is equal to 8 wt% (i.e. 5(10)Fe/8Ba/Al). For these samples, even the surface uptakes more SO_x than conventional 8Ba/Al system, NO_x uptake properties as well as thermal regeneration properties seem slightly improved. On the other hand, for higher Ba loadings (i.e. 5(10)Fe/20Ba/Al) Fe promotion has a minor positive effect on NO_x uptake capacity and SO_x tolerance for 5 wt% Fe promotion while 10 wt% Fe promotion seems to have no positive influence.

5 REFERENCES

[1] http://en.wikipedia.org/wiki/Fossil_fuel

[2] Matsumoto**, S.** *Catalysis Today*, **2004**, 4, 183.

[3] "Emission Control Technologies and the Euro 5/6 Emission Legislation", AECC, http://www.aecc.be/en/Publications/Publications.html.

[4] Birgersson, H. ; Boutonnet, M.; Klingstedt, F.; Murzin, D.Y.; Stefanov, P.; Naydenov, A. *App. Catal. B*, **2006,** *65*, 86.

[5] Burch, R.; Breen, J.P.; Meunier, F.C. *App. Catal. B*, **2002,** *39*, 283.

[6] Matsumoto, S. *Cattech*, **2000,** *4*, 102.

[7] Klingstedt, F.; Arve, K.; Eränen, K.; Murzin, D.Y. *Acc. Chem. Res.*, **2006,** *4*, 273.

[8] Koebel, M.; Media, G.; Elsener, M.; *Catal. Today*, **2002,** *73*, 239.

[9] Klingstedt, F.; Arve, K.; Eränen, K.; Murzin, D.Y. *Acc. Chem. Res.*, **2006,** *4*, 273.

[10] Matsumoto, S.I.; Ikeda, Y.; Suzuki, H.; Ogai, M.; Miyoshi, N.; App. Catal. B, **2000,** 25, 115.

[11] Epling, W.S.; Campbell, L.E.; Yezerets, A.; Currier, N.W.; Parks, J.E. *Catal. Reviews*, **2004**, *46*, 163.

[12] Szailer, T.; Kwak, J.H.; Kim, D.H.; Hanson J.C.; Peden, C.H.F.; Szanyi, J. *Journal of Catalysis*, **2006,** *239*, 51.

[13] Cooper, B.J.; Jung H.J.; Thoss, J.E. U.S Patent 4902487, **1990**.

[14] Xu, J.; Clayton, R.; Balakotaiah, V.; Harold, M.P. *App. Catal. B*, **2008,** *77*, 395.

[15] Fornasari, G.; Trifirò, F.; Vaccari, A.; Prinetto, F.; Ghiotti, G.; Centi, G. *Catal. Today*, **2002,** *75*, 421.

[16] Karlsen, E. J.; Nygren, M. A.; Pettersson, L.G.M. *J. Phys. Chem. A*, **2002,** *106*, 7868.

[17] Cant, N.W.; Patterson, M.J. *Catal. Today*, **2002,** *73*, 271.

[18] Olsson, L.; Westerberg, B.; Persson, H.; Fridell, E.; Skoglundh, M.; Andersson, B. J. *Phys. Chem. B*, **1999**, *103*, 10433.

[19] Cai, S. H.; Rashkeev, S.N., Pantelides, S.T., Sohlberg, K. *Physical Review B,* **2003,** *67,* 224104.

[20] Happel, M.; Desikusumastuti, A.; Sobota, M.; Laurin, M.; Libuda, J. *J. Phys. Chem. C,* **2010**, *114*, 4568

[21] Matsumoto, S. *Catal. Today,* **2004,** *90,* 183.

[22] Tanaka, T.; Tajima, I.; Kato, Y.; Nishihara, Y.; Shinjoh, H. *App. Catal. B,* **2011,** *102,* 620.

[23] Wang, Q.; Zhu, J.; Wei, S.; Chung, J.S.; Guo, Z. *Ind. Eng. Chem. Res.,* **2010,** *49,* 7330

[24] Basile, F.; Fornasari, G.; Grimandi, A.; Livi, M.; Vaccari, A. *App. Catal. B,* **2006,** *69,* 58.

[25] Haruo, I.; Takahashi, N.; Tanaka, T.; Matsunaga, S.; Shinjog, H. *App. Catal. B,* **2009,** *92,* 23.

[26] Hodjati, S.; Petit, C.; Pitchon, V.; Kiennemann, A. *Appl. Catal. B,* **2001,** *30,* 247.

[27] Hepburn, J.S.; Watkins, W.L.H., US Patent 5758489, **1998.**

[28] Yamazaki, K.; Suzuki, T.; Takahashi, N.; Yokota, K.; Sugiura, M. *Appl. Catal. B,* **2001**, *30,* 459.

[29] Fanson, P.T.; Horton, M.R.; Delgass, W.N.; Lauterbach, J. *Appl. Catal. B,* **2003,** *46,* 393.

[30] Hendershot, R.J.; Fanson, P.T.; Snively, C.M.; Lauterbach, *J. Angew. Chem Int. Ed.,* **2003**, *42,* 1152.

[31] Hendershot, R.J.; Rogers, W.B.; Snively, C.M.; Ogunnaike, B.A.; Lauterbach, J. *Catal.Today,* **2004,** *98*, 375

[32] Phuc, N.L.; Courtois, X.; Can, F.; Royer, S.; Marecot, P.; Duprez, D. *Appl. Catal. B,* **2011,** *102,* 353.

[33] Li, X.; Lin, P.; Meng, M. *Catalysis Communications,* **2004,** *5*, 25.

[34] Xian, H.; Zhang, X.; Li, X.; Li, L.; Zou, H.; Meng, M.; Li, Q.; Tan, Y.; Tsubaki, N. *J. Phys. Chem. C,* **2010,** *114*, 11844.

[35] Shen, B.; Liu, T.; Zhao, N.; Yang, X.; Deng, L. *Journal of Environmental Sciences,* **2010,** *22,* 1447.

[36] Rodriguez, J.A.; Jirsak, T.; Gonzalez, L.; Evans, J.; Perez, M.; Maiti, A. *J. Chem. Phys.,* **2001,** *115*, 10914.

[37] Fu, H.; Wang, X.; Wu, H.; Yin, Y.; Chen, J. *J. Phys. Chem. C*, **2007**, *111*, 6077

[38] Baltrusaitis, J.; Cwiertny, D.M.; Grassian, V.H. *Phys. Chem. Chem. Phys.*, **2007,** *9*, 5542.

[39] Decyk, P.; Kim, D.K.; Woo, S.I. *Journal of Catalysis*, **2001,** *203*, 369.

[40] Ertl, G.; Knözinger, H.; Weitkamp, J.; *Preparation of solid catalysts; Inorganic Supports and Catalysts*; Ertl, G., Ed.; Smith, K. Ed.; Wiley-VCH: **1999**

[41] Kayhan, E.; *Structure and NO_x uptake properties of Fe-Ba/Al_2O_3 as a model NO_x storage material;* Bilkent University: **2009**

[42] Karge, H. G.; Dalla Lana, I. G. *J. Phys.; Chem.*, **1984**, *88*, 1538.

[43] Chang, C. C. *J. Catal,*. **1978**, *53*, 374.

[44] Abdulhamid, H.; Fridell, E.; Dawody, J.; Skoglundh, M., *J. Catal.*, **2006,** *241*, 200

[45] Saur, O.; Bensitel, M.; Mohammed Saad, A. B.; Lavalley, J. C.; Tripp, C. P.; Morrow, B. A., *J. Catal,*. **1986**, *99*, 104.

[46] Şentürk, G.S; Vovk, E.I.; Zaikovskii, V.I.; Bukhtiyarov, V.I.; Özensoy, E. *submitted for publication.*

[47] Yamaguchi, T.; Jin, T.; Tanabe, K. *J. Phys. Chem.* **1986**, *90*, 3148.

[48] Yao, H.C.; Stepien, H.K.; Gandhi, H. S. *J. Catal.* **1981**, *67*, 231.

[49] Stakheev, A.Yu.; Gabrielsson, P.; Gekas, I.; Teleguina, N.S.; Bragina, G.O.; Tolkachev, N.N.; Baeva, G.N. *Top. Catal.*, **2007**, *143*, 42.

[50] Hirata, H.; Hachisuka, I.; Ikeda, Y.; Tsuji, S.; Matsumoto, S., *Top.Catal.* **2001**, *145*, 16

[51] Sedlmair, C.; Seshan, K.; Jentys, A.; Lercher, J.A. *Catal. Today* **2002**, *75*, 413.

[52] Waqif, M.; Lavelly, J.C.; Perathoner, S.; Centi, G., *J. Phys. Chem.*, **1991**, *95*, 4051.

[53] Davydov, A.A. Molecular spectroscopy of oxide catalyst surfaces, Wiley, Chichester, England, **2003**.

[54] Datta, A.; Cavel, R.G.; Tower, R.W.; George, Z.M. *J. Phys. Chem.* **1985**, *89*, 443.

[55] http://www.hbcpnetbase.com/

[56] Luo, J-Y.; Meng, M.; Zha, Y.; Xie, Ya-N.; Hu, T.-D.; Zhang J., Liu, T. *Appl. Catal. B* ***2008****, 78,* 38.

[57] Garcia, F.J.; Guerrero, S.; Wolf, E.E.; Miller, J.T.; Kropf, A.J. *J. Catal.* **2005**, *233,* 372.

[58] Uy, D.; Wiegand, K.A.; O'Neill, A.E.; Dearth, M.A.; Weber, W.H. *J. Phys.Chem. B* **2002,** *106,* 387.

[59] Liu, Z.; Anderson, J.A. *J. Catal.* **2004,** *228,* 243.

[60] Kayhan, E.; Andonova, S.M.; Şentürk, G.S.; Chusuei, C. C.; Ozensoy, E., *J. Phys. Chem. C,* **2010**, *114*, 357.

[61] Szanyi, J.; Kwak, J.H.; Kim, D.H.; Wang, X.; Chimentao, R.; Hanson, J.; Epling, W.S.; Peden, C.H.F. *J. Phys. Chem. C* **2007**, *111*, 4678.

[62] Kwak, J. H.; Mei, D.; Yi, Ch.-W.; Kim, D. H.; Peden, C. H. F.; Allard, F. *J. Catal.* **2009**, *261*, 17.

[63] Digne, M.; Sautet, P.; Raybaud, P.; Euzen, P.; Toulhoat, H. *J. Catal.* **2004**, *226*, 54

[64] Venkov, T.; Hadjiivanov, K.; Klissurski, D. *Phys. Chem. Chem.Phys.* **2002**, *4*, 2443

[65] Szanyi, J.; Kwak, J. H.; Kim, D. H.; Burton, S. D.; Peden, C. H. F. *J. Phys. Chem. B* **2005**, *109*, 27.

[66] Kwak, J. H.; Hu, J. Z.; Kim, D. H.; Szanyi, J.; Peden, C. H. F. *J. Catal.* **2007**, *251*,189.

[67] Ozensoy, E.; Herling, D.; Szanyi, J. *Catal. Today* **2008**, *136*, 46.

[68] Pacchioni, G.; Clotet, A.; Ricart, J. M. *Surface Science* **1994,** *315,* 337.

[69] Goodman, A.L.; Li, P.; Usher, C. R.; Grassian, V. H. *J. Phys. Chem. A* **2001,** *105,*6109